Lund University GEM thesis series nr 27

Conflict, narratives, and forest fires in eastern Turkey

A quantitative perspective with remote sensing and GIS

Aiman Shahpurwala

2019
Department of Physical Geography and Ecosystem Science
Lund University
Sölvegatan 12
S-223 62 Lund
Sweden

LUND UNIVERSITY

UNIVERSITY OF TWENTE.
FACULTY OF GEO-INFORMATION SCIENCE AND EARTH OBSERVATION

CONFLICT, NARRATIVES, AND FOREST FIRES IN EASTERN TURKEY

A QUANTITATIVE PERSPECTIVE WITH REMOTE SENSING AND GIS

by
Aiman Shahpurwala

Thesis submitted to the department of Physical Geography and Ecosystem Science, Lund University, in partial fulfilment of the requirements for the degree of Master of Science in Geo-information Science and Earth Observation for Environmental Modelling and Management

Thesis assessment Board

First Supervisor: *Professor,* Petter Pilesjö (Lund University)
Co-supervisors: *Marie Curie Fellow,* Pinar Dinc (Lund University) and *Assistant Professor*, Lina Eklund (Aalborg University)

Exam committee:
Examiner 1: Jonathan Seaquist
Examiner 2: Ali Mansourian

Disclaimer

This document describes work undertaken as part of a program of study at the University of Lund. All views and opinions expressed therein remain the sole responsibility of the author, and do not necessarily represent those of the institute.

Course title: Geo-information Science and Earth Observation for Environmental Modelling and Management (GEM)

Level: Master of Science (MSc)

Course duration: January 2019 until June 2019

Consortium partners:

The GEM master program is a cooperation of departments at 5 different universities:
University of Twente, ITC (The Netherlands)
University of Lund (Sweden)
University of Southampton (UK)
University of Warsaw (Poland)
University of Iceland (Iceland)

Abstract

Conflict, Narratives and Forest Fires in Eastern Turkey
by Aiman Shahpurwala

Keywords: wildfire, warfare ecology, burned area, fire detection, multi-temporal analysis, quantitative assessment, Tunceli, Turkey

Within Turkey, claims of an increasing number of forest fires ignited by the Turkish military to 'strategically degrade the environment' broke out after the Turkish-Kurdish peace process ended in 2015. These claims are built on little evidence, and fire occurrences are not well documented. Yet, the issue has gained attention through the news and social media in recent years (Nurcan Baysal 2018; Stockholm Center for Freedom 2018). The lack of objective, scientific, data presents a need for a quantitative assessment of these fires in the context of conflict and political instability. Modern techniques in remote sensing and GIS can be used to retrospectively account for these fires. The research uses a multi-temporal/ multi-scale approach provided in three parts, including: 1) the characterization of alleged fires (from 2016 to 2018) at a local scale, 2) assessment and validation of 9 years of fire data on the provincial scale and, 3) statistical analysis and hypothesis testing (i.e., Spearman Rank Correlation Test) for the association between 15 years of fire and conflict data at the national/provincial scale. Parts one and two focus on Tunceli Province at the local and provincial scale, and part three focuses on analyzing fire accounts from Diyarbakir, Hakkari, and Tunceli provinces against Turkey's national conflict data. In part one, a relativized burn ratio (i.e., RBR) was calculated to determine fire severity, and 77% of the burned area identified as low severity burns (USGS 2004). In part two, trends showed increases in fires and burned area after the year 2015, and the fire product validation found an overall map accuracy of > 90%. Part three determined a statistically significant association between the conflict and fire data in all three provinces. Results from these experiments show that modern techniques in remote sensing are useful for quantitative assessments of fire patterns within the context of conflict and political instability. Furthermore, the remote sensing data partially supports local claims that the fires are occurring and have increased after the year 2015.

Acknowledgments

‘If I have seen further it is by standing on the shoulders of giants’ – Isaac Newton (1675)

Firstly, I would like to thank my family for always supporting me and encouraging me to go on this journey to Europe for higher studies.

Thank you to the FIRE team, Pinar Dinc, Petter Pilesjö, and Lina Eklund for providing me with this exciting research opportunity and helping me to grow in my career.

I want to express my gratitude for the kind hospitality of the local people I met in Tunceli. I want to thank Irem Aydemir along with the people that helped me while I was there; your experiences helped me to understand the complexities of the war and the vulnerability of the environment. It was an eye-opener.

Additional thanks to David Tenenbaum, Virginia Garcia, and Hanna Glad for their encouragement in the learning process and helpful advice. I would also like to give notice to the Earth Observation Group for the opportunity to present my results and express my confusion and get useful feedback.

To my friends at Lund University, thank you for helping me to relax and enjoy this experience, so happy to have met you all. To my friends at ITC, my comrades, I learned so much from you all; glad we made it through those hard days together! A very special thanks to Felipe Fonseca, Stephanie Elizabeth Judge, Tom Albin Tveitan Käppi, Camilla Persson, Alexandra Pongracz, and Lone Mokkenstorm I could not have done it without you guys!

Abbreviations

Active Fire (AF)
Application for Extracting and Exploring Analysis Ready Samples (AppEEARS)
Burned Area (BA)
delta Normalized Burn Ratio (dNBR)
European Space Agency (ESA)
Fighting Insurgency, Ruining the Environment (FIRE)
Geographical Information Systems (GIS)
Georeferenced Event Dataset (GED)
Global Fire Emissions Database (GFED)
Kurdistan's Workers Party (PKK)
Mid-Infrared (MIR)
Moderate Resolution Imaging Spectrometer (MODIS)
Near-Infrared (NIR)
Normalized Burned Ratio (NBR)
Normalized Difference Water Index (NDWI)
Quality Assessment (QA)
Relativized Burn Ratio (RBR)
Sentinel Application Platform (SNAP)
Shortwave-Infrared (SWIR)
The National Aeronautics and Space Administration (NASA)
United States Geological Survey (USGS)
Universal Transverse Mercator (UTM)
Uppsala Conflict Database Program (UCDP)
Vegetation Index (VI)
Visible Infrared Imaging Radiometer Suite (VIIRS)

TABLE OF CONTENTS

1. INTRODUCTION

This thesis combines political studies, physical geography, and geomatics to address a real-world problem regarding the claims of the 'purposeful burning of forest to strategically degrade the environment' in Turkey after the year 2015 (i.e., the end of the Kurdish-Turkish peace process). The thesis is structured in a way to first introduce the problem and context, and then to explore tools and techniques in remote sensing and geospatial analysis which can be used to help address the problem. Firstly, the context and history of the problem are described in Sections 1.1 and 1.2. Then Sections 1.3 will follow up with the aim, the research questions, and the objectives.

1.1 THE SOCIOPOLITICAL CONTEXT

1.1.1 HISTORY OF KURDISH – TURKISH CONFLICT IN TUNCELI

The fall of the Ottoman Empire after World War I resulted in the splitting of Kurdish communities across Turkey, Syria, Iraq, and Iran. As a result, many Kurdish people ended up in Turkey. In fact, Turkey has the largest Kurdish population making up 19% of its total population (Central Intelligence Agency 2019). The Kurdish people primarily live in eastern/southeastern Turkey, a geographically diverse region with mountainous ecoregions rich in unique flora. Since the Kurdish migration, there has been a high degree of animosity in eastern/southeastern Turkey between the state of Turkey and Kurdish insurgent groups. The Kurdish insurgent groups, such as the Kurdistan Worker's Party (PKK) (established in 1978) have been demanding for the creation of an independent state of Turkish Kurdistan or to have autonomy including political and cultural rights for Kurds within the Republic of Turkey (Ekurd Daily 2011). The battle for Kurdish autonomy has been long and undoubtedly influenced the land systems (i.e., human use of land and the environmental outcomes) of eastern/southeastern Turkey. This paper intends to focus on the influence of the conflict between the PKK and Turkish State on land systems in more recent history (i.e., 1978 to present).

The recent history of the PKK-Turkish conflict can be traced back to 1978 when the state of Turkey declared martial law (Dahlman 2008). This event prompted the PKK to initiate guerrilla warfare against the state of Turkey in 1984 (Dahlman 2008). Even though the PKK were outnumbered, the Turkish Army performed poorly against the guerillas and the PKK were able to maintain dominance over large areas in eastern/southeastern Turkey by 1990 (Jongerden et al. 2007). However, in 1993, the Turkish Army completed what is known as the 'field domination doctrine' aimed to establish area control by a 'clear and hold' strategy (Jongerden et al. 2007). As part of the new strategy, the doctrine prioritized the destruction of the PKK's environment, which included systematic village evacuations and the destruction and burning of forests (Jongerden et al. 2007). Village evacuations took place between 1990 and 1995. 1994 accounted

for the most village evacuations, with a reported 1,334 evacuated or destroyed villages (Amnesty International 1994). Tunceli Province, a mountainous region located in eastern Turkey, was a primary target since many PKK members used the mountains in the region as a hiding place. A local politician claimed that 25% of the forest in Tunceli was destroyed at that time (SNK 1994). However, human rights organizations were not able to evaluate the extent of human rights violations because the military sealed off affected areas (Jongerden et al. 2007).

After the devastating village evacuations and forest burnings in the mid-1990s the Kurdish population decreased by 35% in the year 2000 (Jongerden et al. 2007). In 1999, after PKK leader Abdullah Ocalan was captured, the PKK declared a unilateral ceasefire until 2004 (Balta 2005). The end of the ceasefire in 2004 led to a rise in conflict which remained ongoing until 2008. In 2009 the 'Kurdish or Democratic Opening' a peace initiative, led to a decline in conflict until 2010. However, due to tension from the Syrian War, violent conflict increased in 2011 and 2012, with the number of deaths tolling higher than the previous years (International Crisis Group 2012). In 2013, a ceasefire was declared, and peace talks proceeded between the Turkish government and PKK with the intent to create a peace process known as the 'Solution Process'. The truce was working until PKK members shot two police officers on July 22nd, 2015, causing an escalation of violence and ending the peace process (Köse 2017). Consequently, full-scale warfare was renewed in eastern/southeastern Turkey with the conflict ongoing to the present day (i.e., 2019) (Crisis Group 2019). To summarize, Figure 1.1 provides a timeline of events of the PKK-Turkish conflict from 1978 to the present day. Years in red show periods of heightened violence and years in blue describe periods of ceasefire or peace negotiations.

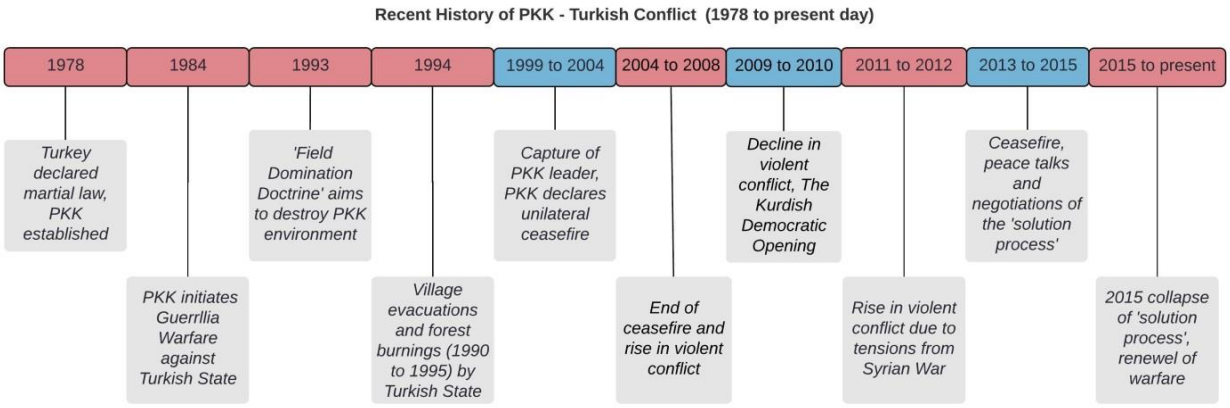

FIGURE 1.1 HISTORY OF PKK-TURKISH CONFLICT FROM 1978 TO PRESENT (2019)

1.1.2 *Conflict and Forest Fires in Tunceli*

Figure 1.2 Tweet from an environmental NGO (i.e., @350ankara) on the destruction of nature in Tunceli

Figure 1.3 Tweets by Media Investigation Organization (i.e.,@gununyalanlari) falsifying a claim posted on Twitter, noting the image is from a wildfire abroad

The ongoing conflict and tension between Kurdish insurgent groups and the Turkish state have threatened the lives and livelihood of many civilians living in eastern/southeastern Turkey. In particular, the traumatic memory of the village evacuations and forest burnings in Tunceli between 1990 and 1995 are still carried by the remaining locals (Jongerden 2010; Tekinoğlu 2017). After the collapse of the 'Solution Process' in 2015, the renewed strife once again threatens the local people's security and environment. Claims of wildfires running rampant in the region during the yearly dry seasons have caught attention in the media in recent years (i.e., May to October) (HDP 2015).

Local people, non-governmental organizations, and various actors claim that Turkish state is once again setting the forests on fire to destroy the environment, and cause people to leave their homes (HDP 2015), with the most recent claims in August 2018 (350 Ankara 2018; Stockholm Center for Freedom 2018). Affected civilians claim that they have little help from authorities in putting out the fires and instead tried to put the fires out themselves (HDP 2015). Many used the Twitter hashtag '#dersimyanıyor' (i.e., 'Dersim on Fire') to raise awareness of the issue online (Figure

1.2) (350 Ankara 2018). Similar claims in Diyarbakir and Hakkari, provinces well-known in the PKK-Turkish conflict, also arose in recent years, but are not as well known in social media (HDP 2015). Despite the outcry, these claims are built on little evidence because the fires are not well documented. Incidentally, the Turkish government does admit in a press release in August 2017 that fires between Hozat-Alibogazi, Center-Kutuderesi, and Munzur Valley-Bali Creek in Tunceli Province were started due to violent conflict with terrorist organizations and were not extinguished immediately due to ongoing operations (TC Tunceli Governorship 2017). Nonetheless, as for that exception, the Turkish government did comment that many of the allegations are false and the reports in the media often contain pictures that are not even from Tunceli Province (Tunceli Governor 2018). Furthermore, organizations investigating claims on social media reported imagery falsely used to support claims, such as, images of fires elsewhere (see Figure 1.3), and outdated imagery being used (Yalanlari 2017; teyit 2018). These indeterminate and disputed accounts of forest fires in Tunceli, as well as in the provinces of Diyarbakir and Hakkari, presents a need for objective and quantitative research in these areas. The research should account for the fires, the fire severity or impact, and also address the forest fires within the context of conflict presented by these narratives.

1.2 The Academic Context

Currently, there is an extensive research gap regarding the effect of conflict on forest systems. However, there are a few broader studies and frameworks which are useful for assessing the ecological impacts of conflict. One framework is known as 'warfare ecology' put forth by Machlis and Hanson (2008). The concept of warfare ecology and a few existing studies on forests systems affected by conflict are explained in the following section as well as the potential use of remote sensing and geographical information systems (GIS) within this research field.

1.2.1 Warfare Ecology

While the link between climate change and natural resource degradation as a driver of conflict has been readily explored (Adger et al. 2014), research regarding conflict as a driver of environmental degradation is limited (Machlis and Hanson 2008; Baumann and Kuemmerle 2016). To address this large research gap, Machlis and Hanson (2008) outlined a field of study called 'warfare ecology'. The authors divided the stages of warfare into 1) preparations for war, 2) war (violent conflict), and 3) postwar activities, with each stage generating various ecological consequences.

With regards to forest systems, the second stage of warfare, war (violent conflict), often results in forest loss and degradation. Baumann and Kuemmerle (2016) found that out of the 16 studies

analyzing forest change with regards to conflict, 12 of them found forest loss, which was typically caused directly by the fighting (e.g., defoliating agents, fires, bombing…). Since insurgent groups tend to hide out in forest systems, counterinsurgency strategies can specifically target these forest systems in an effort to destroy the enemy. A well-known example of this is Turkey's counterinsurgency measures against the PKK in the mid-1990s described in Section 1.1 (Jongerden et al. 2007; Hanson 2018).

Unfortunately, the limited number of studies surrounding the topic of forests and conflict make it difficult to fully understand the effects of conflict on forest systems (Camilla et al. 2008). Baumann and Kuemmerle (2016) identify the need for more empirical and quantitative case studies between conflict data and land use/ land cover change to understand the large scale effects of conflict on forest systems. Machlis and Hanson (2008), call for in-depth case-studies of the impact of warfare on the environment, with a focus in empirical analysis. Additionally, the recognition of an interdisciplinary approach grounded in quantitative spatial analysis is also acknowledged by many (Camilla et al. 2008; Machlis and Hanson 2008; Baumann and Kuemmerle 2016; Hanson 2018).

Considering the need for more quantitative case studies in warfare ecology, remote sensing presents an effective tool set to carry out quantitative spatial analysis for investigating the impact of conflict on forest systems (Chuvieco 2009). For example, retrospective forest fire investigation and detection is possible with remotely sensed archived data providing an alternative method to field investigation. Using remote sensing data, modern techniques are able to detect the number of fires, accurately predict the date of burning, measure total burned area, assess fire severity, and even assess the damages and extent of destruction (Melorose et al. 2015). These techniques are particularly useful for investigating past fires and fires in areas of limited accessibility such as conflict zones.

1.3 FIRE: The Project and The Master's Thesis Research

This thesis paper introduces an initial case study for Fighting Insurgency, Ruining Environment or FIRE (https://fireproject.blog/), a Marie Sklodowska-Curie Actions project, which addresses the research gap between conflict and forest fires by planning in-depth investigations within the Middle East. In particular, this thesis project focuses on the relationship between conflict and fires within Turkey with specific interest in the disputed region of modern-day Tunceli Province, also known as 'Dersim'. The focus on Tunceli will highlight an ongoing narrative, which first gained attention in 2015, of locals claiming that the state of Turkey is purposefully setting their forests on fire (Stockholm Center for Freedom 2018). The provinces of Diyarbakir and Hakkari, also well-known in the PKK-Turkish conflict, are also explored in part.

1.3.1 THE AIM AND RESEARCH QUESTIONS

This MSc thesis project aims to explore and determine useful techniques to characterize and account for forest fires remotely, as well as to explore data and methods to assess the link between reports of violent conflict and fires. The fire and conflict data are qualitatively analyzed with respect to the ongoing narratives, and within the context of fluctuating political instability and conflict (i.e., PKK-Turkish War). The research focuses on the more recent events of the PKK-Turkish War from the early 2000s to 2018. The research is conducted in three parts; starting with the smallest spatial and temporal scale and sequentially widening to the largest (see Figure 1.4).

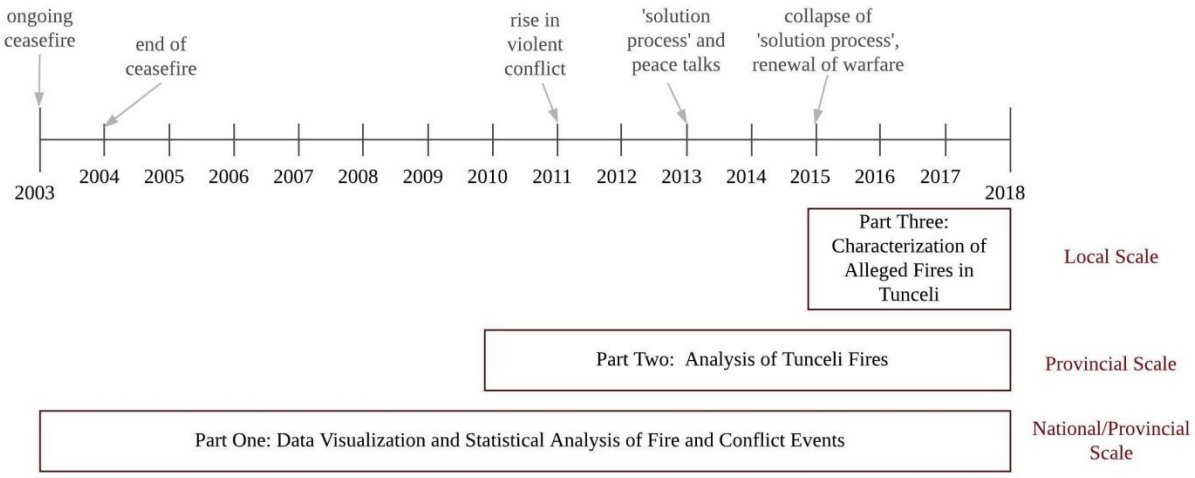

FIGURE 1.4 ILLUSTRATION OF THE TIMELINE AND SCALE(S) USED IN EACH OF THE THREE PHASES OF THE RESEARCH

For each part, spatial data and techniques in remote sensing and geographic information systems (GIS) are explored and used in quantitative assessments. The results will be used to refine methods for future work and to contribute any relevant, objective findings to the FIRE project. Each part of the research corresponds to the following three research questions and related objectives in order:

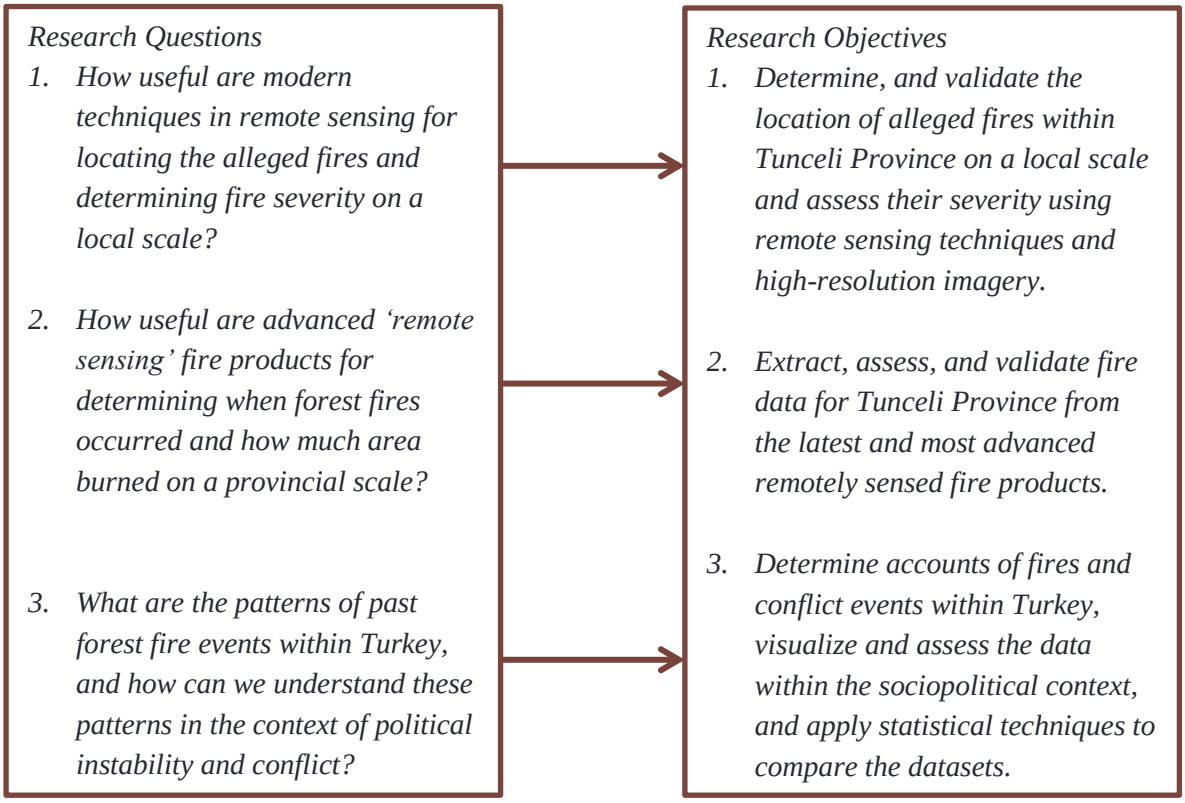

2. BACKGROUND

1.1 ROLE OF REMOTE SENSING AND GIS IN FIRE INVESTIGATION

Remote sensing refers to the acquisition of information about the physical characteristics of Earth's landscapes and phenomena by detecting and monitoring reflected or emitted radiation from the surface (USGS 2019). There are two primary remote sensing instruments, active and passive sensors. These sensors are situated onboard satellites and look down at the Earth's surface as the satellite's orbit around Earth. Active sensors (i.e., radar, laser scanners) work by directly sourcing energy down to the surface and measuring the radiation reflected back up. On the other hand, passive sensors (i.e., radiometers, spectroradiometers) detect radiation naturally emitted by the Earth's surface or reflected by the sun. Any and all radiation detected by these sensors fall within the electromagnetic spectrum. This reflected radiation is often expressed as spectral reflectance, which describes the portion of incident radiation (i.e., sunlight) reflected as a function of wavelength (i.e., expressed as a ratio, and therefore independent of illumination). For each subject of interest (i.e., vegetation, soil, burned areas…) a spectral reflectance curve may be generated which describes the average spectral reflectance for that subject in each section of the electromagnetic spectrum.

Figure 2.1, from Quayle (2010), shows the typical spectral response curves of healthy vegetation and burned area. The largest difference between healthy vegetation and burned area is observed in the near-infrared and short-wave infrared wavelengths.

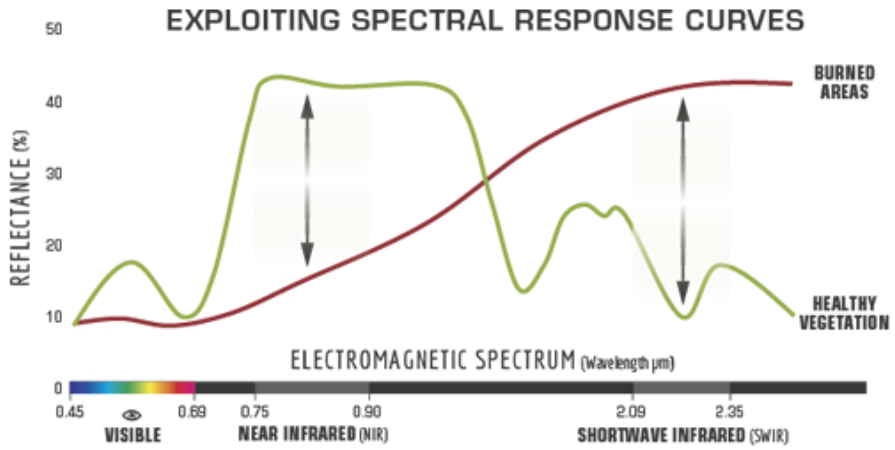

FIGURE 2.1 DIAGRAM FOR SPECTRAL RESPONSE CURVES OF HEALTHY VEGETATION AND BURNED AREAS BY THE UNITED STATES FOREST SERVICE (QUAYLE ET AL. 2010)

Passive sensors are primarily used for fire detection purposes. Within the use of passive sensors, two types of fire sensing techniques are found, active and passive. These should not be confused with the active and passive remote sensing instruments previously described. The two fire sensing techniques are described below.

ACTIVE FIRE SENSING

Active fire sensing relies on thermal infrared (i.e., long-wavelength infrared) emissions from the Earth's surface to detect thermal anomalies or hotspots, which can indicate the presence of fires. This type of sensing does not rely on reflected sunlight, but rather heat emitted from the Earth's surface. In fire detection, thermal anomalies describe temperature differentiation between the ongoing fire and the surrounding area. For example, a grassland fire may burn at 800 K showing a peak radiance between 3 and 5 µm (San-Miguel-Ayanz et al. 2005). This peak in radiance can be separated from the normal background radiance or Earth's ambient temperature (300 K) to identify a hotspot (Wooster et al. 2013).

The advantage of active fire sensing over conventional surface reflectance sensors is the ability to detect thermal signals day or night, as no sunlight is needed. Additionally, thermal data is useful in removing interference from clouds and cloud shadows (Giglio et al. 2003). Active fire sensing allows for real-time data collection of current fires, and the archived data can be used retrospectively. Furthermore, while small fires (e.g., 2 m^2) can be detected, the exact location is difficult to pinpoint as data is aggregated in larger pixels (i.e., image elements of 500 m^2). Still, this technique is often used in forest fire research to help locate or approximate burned areas (San-Miguel-Ayanz et al. 2005; Schroeder and Giglio 2016; Chuvieco et al. 2018; Giglio et al. 2018b).

PASSIVE FIRE SENSING

In the detection of burned areas, passive fire sensing relies on prompt changes in reflected radiation. This can be observed as a forest's bright green foliage burning up and leaving behind a dark area of brown tree poles and black char. Since the burning needs to have already occurred for the detection to take place, passive sensing can only detect past fires. Passive sensing is useful in post-fire investigation as it allows for fire perimeters to be drawn and total burned area to be calculated. However, passive sensing is limited by poor visibility due to smoke, cloud, and cloud shadow interference, making large areas of data inaccessible. Passive fire sensing relies on changes within the visible, near-infrared (NIR), mid-infrared (MIR), and shortwave infrared (SWIR) wavelengths as opposed to active fire sensing which relies on thermal wavelengths. While active and passive fire sensing techniques are useful independently, the combination of the two techniques is highly desirable for fire characterization (Giglio et al. 2018b).

2.1.1 Change Detection Algorithms For Burned Area Mapping

Robust change detection algorithms combine active and passive fire sensing methods to extract burned area from satellite data. These algorithms are used on a time sequence of images (Achard and Hansen 2017). Depending on the number of images available, images may be organized as a time series stack (e.g., images obtained daily) or pre- and post-fire disturbance images may be manually selected (e.g., images obtained monthly).

Typically, fire detection algorithms make use of spectral reflectance data to calculate relevant descriptive indices. These indices are derived from changes in spectral reflectance of multiple band combinations typically formulated in a simple equation (see Eq. 1). Common fire-related indices include the 'Normalized Burned Ratio' (NBR) and the 'Burned Area Index' (BAI). These types of indices can be used in the quantification of fire severity and burned area (Melorose et al. 2015). The severity of the fire or burn severity is used to describe the overall degree of impact from all the combined fire effects (Eidenshink et al. 2007). The indices are calculated for each image selected and differenced to understand the changes over time, a technique called image differencing. For example, the NBR exploits the fact that burned areas have lower NIR and higher SWIR reflectance values compared to healthy vegetation (see Eq.1) (Key and Benson 2006). A higher NBR value indicates healthy vegetation, while a lower NBR typically indicates bare ground or areas of recent burning (Key and Benson 2006).

Eq.1 $$\mathrm{NBR} = (\mathrm{NIR} - \mathrm{SWIR}) \div (\mathrm{NIR} + \mathrm{SWIR})$$

After image differencing, active fire sensing is often used to spatially and temporally constrain the burned area and burn date (Giglio et al. 2018b). The higher temporal resolution also aids in establishing the origin and understanding the growth of the fire.

3. STUDY AREA

The disputed region of Tunceli Province is of primary focus of this research, and is known as the case study area. However, Diyarbakir, and Hakkari at the provincial scale and Turkey at the national scale (see Figure 3.1) are also explored with Tunceli in the last part of the thesis. The provinces selected are well-known areas in the PKK-Turkish conflict.

FIGURE 3.1 MAP OF TURKEY WITH PROVINCES OF INTEREST HIGHLIGHTED IN COLORS. **INSET:** MAP OF TUNCELI PROVINCE OUTLINED IN PINK. ADMINISTRATIVE BOUNDARY DATA DOWNLOADED FROM THE HUMANITARIAN DATA EXCHANGE (REGIONAL IM WORKING GROUP - EUROPE 2019). BASE MAPS BY ESRI WORLD MAPS.

3.1 TURKEY

Turkey is a transcontinental country joining Europe and Asia, with a population of 81 million (Central Intelligence Agency 2019). Turkey's 783,562 km^2 expanse is known for its geographically diverse mountainous landscapes with unique biodiversity (Central Intelligence Agency 2019). The Koroglu and Pontic mountain ranges lie in the north, and the Taurus Mountain's in the south. Turkey is also home to the source waters of the historic Euphrates,

Tigris, and Aras rivers. There are seven geographical regions from west to east: Marmara, Aegean, Mediterranean, Central Anatolia, Black Sea, Southeastern Anatolia, and Eastern Anatolia. Turkey has four seasons: summer (June, July, August), winter (December, January, February), spring (March, April, May), and autumn (September, October, November). Turkey's western and southwestern regions have a temperate Mediterranean climate while the eastern regions have a continental climate with severe winters and hot and dry summers (Central Intelligence Agency 2019).

3.2 HAKKARI PROVINCE

Hakkari Province is located in Southeastern Anatolia, in the most southeastern point of Turkey, bordering Iran. The province consists of a 7,121 km^2 area and has a population of 251,302 (T.C. Hakkari Governorship 2019). The landscape is shaped by the Taurus Mountains. While Hakkari has more severe winter conditions in the higher altitudes, the climate in the valleys is milder. The temperatures range from an average of 24°C in the summer months to -3.8°C in the winter (climate-data.org 2019). The wet season is during winter/spring, and the dry season is during summer/autumn. Average monthly rainfall during the wet season is 113 mm and 8 mm during the dry season (climate-data.org 2019). Valley slopes are covered with oak forests and flat areas are covered with walnut and mulberry trees. Forest makes up 20% of the land cover in Hakkari (Eroglu and Üzmez 2015).

3.3 DIYARBAKIR PROVINCE

Diyarbakir Province is also located in Southeastern Anatolia. The province has a surface area of 15,355 km^2 with a population of 1,732,396 (Turkish Statistical Institute 2018). Diyarbakir has a continental climate with hot and dry summers and mild winters (Baran et al. 2011). The temperature ranges from an average of 29°C in the summer and 2.2°C in the winter (climate-data.org 2019). The wet season is during winter/spring, and the dry season is during summer/autumn. Average monthly rainfall during the wet season is 76 mm and 3 mm during the dry season (climate-data.org 2019). Diyarbakir is relatively flat compared with the other provinces of interest. Forest cover makes up 24.4% of the land (Eroglu and Üzmez 2015). The city of Diyarbakir is the largest city in southeastern Turkey and is situated on the banks of the Tigris River. It is a major cultural hub for Turkey's Kurdish population (The Kurdish Project 2019). Diyarbakir is also well known for its historical civilizations and holds many UNESCO world heritage sites (UNESCO World Heritage Centre 2015).

3.4 TUNCELI PROVINCE (CASE STUDY AREA)

Tunceli Province, known as 'Dersim' by the locals, is situated in Eastern Anatolia. The province encompasses a 7,774 km^2 area and is home to the Munzur Mountains and the Munzur catchment,

a primary tributary to the Euphrates River (TC Tunceli Governorship 2019). Tunceli has a continental climate, known for its extreme seasonal temperature differences, with an average of -2°C in the winter and an average of 26°C in summer (climate-data.org 2019). The wet season is during winter/spring, and the dry season is during summer/autumn. Average monthly rainfall during the wet season is 112 mm and 10 mm during the dry season (climate-data.org 2019). Tunceli has a population of 88,198. Agriculture is a primary source of income with animal husbandry and crop farming as the more dominant occupations. Forest cover makes up approximately 29% of the land (Eroglu and Üzmez 2015). The forests are primarily oak-dominated deciduous forests.

Tunceli is also home to Munzur Valley National Park. The park is known to host unique flora and fauna and is home to 1,518 registered species of plants, many of which are endemic to the region (National Parks Of Turkey 2019). The park's forested mountains provide an adequate habitat for wildlife such as mountain goat and wild boar (National Parks Of Turkey 2019). In 2012, the World Wildlife Fund (WWF) deemed the Eastern Anatolian Mountain Range as an ecoregion for its unique biodiversity and landscape. According to the WWF (2019a), an ecoregion is a 'large unit of land or water containing a geographically distinct assemblage of species, natural communities, and environmental conditions'. The WWF gave the ecoregion vulnerable status for environmental degradation (World Wildlife Fund 2019b; World Wildlife Fund 2019a).

FIGURE 3.2 PHOTOGRAPHS OF MUNZUR VALLEY NATIONAL PARK IN TUNCELI. **LEFT:** THE PARK'S MOUNTAINOUS LANDSCAPE AND THE MUNZUR RIVER. **RIGHT**: MOUNTAIN GOAT FORAGING ON THE MOUNTAIN SIDE**.** PHOTOS BY: AIMAN SHAHPURWALA (2019)

4. DATA

The following sections describe in detail the remote sensing and geospatial data used in this research.

4.1 FIRE PRODUCTS

Currently, two of the most reliable global fire data products are the 'Collection 6 (C6) Moderate Resolution Imaging Spectroradiometer (MODIS) Active Fire (AF) and Burned Area (BA) Products' (Fornacca et al. 2017). Data is derived from MODIS instruments aboard satellites Aqua (launched 2001) and Terra (launched 1999). MODIS C6 fire product suite was released in 2017 and improved on the MODIS Collection 5.1 fire products. This collection update is part of a standard periodic reprocessing to incorporate better calibration techniques and algorithm refinements (Giglio et al. 2018b). The MODIS BA and AF products are produced daily at 500 m and 1 km spatial resolutions, respectively (Giglio et al. 2003). NASA's newer Visible Infrared Imaging Radiometer Suite (VIIRS) aboard the Suomi National Polar-orbiting Partnership (Suomi NPP) satellite launched in 2011, complements the MODIS AF products with an improved spatial resolution and greater small fire detection. VIIRS's M-band and I-band, consisting of various radiometric channels, are used in AF detection and produce daily data at 750 m and 375 m spatial resolution, respectively (Schroeder and Giglio 2016).

Specifications of the fire products are detailed in Table 4.1. Sections 4.1.1 to 4.1.3 describe the algorithms used to create them. Furthermore, the internal accuracy assessment and validation is provided as justification for the use of the data product in this research.

4.1.1 MODIS BA ALGORITHM DESCRIPTION AND ACCURACY ASSESSMENT

The C6 MODIS BA product update includes an overall improvement in BA detection and a reduction in errors (Giglio et al. 2018a). The mapping algorithm described in Giglio (2018b) combines 500 m MODIS daily surface reflectance data with 1 km MODIS AF data; resampled to 500 m for consistency. Cloud and water pixels are masked, so they do not interfere with BA detection. The data is atmospherically corrected for true ground reflectance by minimizing the effects of atmospheric scattering. This data is then used to calculate burn-sensitive vegetation indexes (VI) with short-wave infrared (SWIR) channels 5 (ρ_5) and 7 (ρ_7) (see Eq. 2) (see Appendix A, Table 1A for wavelengths).

Eq.2
$$VI = (\rho 5 - \rho 7) / (\rho 5 + \rho 7)$$

Eight consecutive days of VI images and AF data are temporally composited, and sliding windows are used to detect substantial temporal changes of the VI. This technique is similar to image differencing explained in Section 2.1.3, where the differenced values are compared and

the largest differences for each pixel over the eight days are found and summarized in a 'temporal texture' dataset. The 'temporal texture' dataset and AF data are then used for identifying burned and unburned training samples for classification. The supervised classification consists of separability testing and posterior burn probability statistics to derive initial classification. MODIS land cover data is used here to adjust burn thresholds to account for the background's natural variability, and AF data are used to guide the algorithm in estimating burn dates. Subsequently, statistical filtering using contextual or background information is performed to relabel any pixels wrongly classified as 'burned' or 'unburned'. The resulting product is a monthly composited burn mask containing five data layers including burn date, burn date uncertainty, quality assurance, as well as first and last burn date quality detection thresholds (Giglio et al. 2018b). The burn date layer is classified for water (-2), missing data (-1), unburned pixels (0), and burned pixels, where the value of the pixel (1 to 256) is the date-of-burn in Julian Days (JD). This combined use of AF and reflectance data enables the algorithm to adapt regionally over a wide range of pre- and post-burn conditions and across multiple ecosystems (Giglio et al. 2009).

According to Giglio (2018b), validation of the MODIS BA product using globally distributed, high-resolution, Landsat reference data (30 m) resulted in a good agreement between the reference images and classification with a correlation (r^2) of 0.818, a 24% error of commission, and a 37% error of omission. Furthermore, validation of the estimated burn date found 44% of fires were detected on the same day, and 68% of fires were detected within two days. Consequently, the improved algorithm, and the results of the global validation found the MODIS BA product suitable for further analysis in this research.

4.1.2 MODIS AF Algorithm Description and accuracy assessment

C6 MODIS AF product improves on the previous collection by reducing the occurrence of false alarms by small forest clearings and the omission of large fires obscured by smoke (Giglio et al. 2016). The algorithm, described by Giglio (2016), uses MODIS channels 21, 22, and 31 which are the primary mid-infrared to thermal channels used in fire detection (see Appendix A, Table 1A for wavelengths). Cloud and water pixels are masked using temperature thresholds for radiant temperature derived from the spectral radiance measured by channels 1, 2, 31, and 32 (see Appendix A, Table 1A for wavelengths). The pixels not masked out are considered as 'potential fire pixels' and are further analyzed. Next, a moving window is used to characterize the surroundings of a 'potential fire pixel', by averaging temperature values and then using day and night temperature thresholds to search for 'background fire pixels'. After the background characterization, a series of contextual threshold tests are used to search for the unique signature of an active fire, where significant temperature differences are found between 'background fire pixels' and 'non-fire background pixels'. The dynamic thresholds are relative to the background's natural variability. A pixel is tentatively classified as a 'fire pixel' if it successfully

passed specific tests. Finally, pixels flagged as 'fire pixels' go through a series of 'false-alarm rejection tests' to identify other possibilities for the reflectance changes, such as sunglint, forest clearings, and boundaries where land cover changes drastically. The fire pixels that pass all the false-alarm rejection tests are officially classified as 'fire pixels' with a certain confidence of detection, and all other pixels are classified as 'non-fire pixels' (Giglio et al. 2016).
According to Giglio (2016), the MODIS AF product had an overall global omission error of 86.2%, which decreases if the fire size increases. However, for fires approximately > 0.20 km^2 the omission error stabilizes around 5%. MODIS AF also had a daytime commission error of 1.2% and the nighttime commission error was negligible. The improved algorithm and, validation results provide reason enough to deem the MODIS AF product suitable for further analysis in this research.

4.1.3 VIIRS AF Algorithm Description and accuracy assessment

VIIRS AF product complements MODIS AF data by providing a higher resolution product at 375 m. It improves on the detection of small fires and fire perimeter mapping for larger fires (Schroeder and Giglio 2016). As described in Schroeder and Giglio (2016), the product uses a hybrid algorithm which combines VIIRS channel I (1-15) at 375 m resolution and channel M13 at 750 m (see Appendix A, Table 1A for wavelengths). Channel I is primarily used for fire detection, and channel M is used for understanding sub-pixel fire radiative power (FRP), which essentially measures the energy of the fire. The VIIRS algorithm uses a combination of fixed and contextual tests to detect AF and other thermal anomalies in the day and night. The algorithm builds on the Giglio (2016) MODIS AF algorithm (see Section 4.1.2) with some modifications.

As described in Schroeder (2014), VIIRS AF fire pixels are categorized by daytime or nighttime detection with confidence levels of low, nominal, and high. An initial assessment estimated VIIRS AF commission errors for daytime low confidence pixels. Single date high-resolution Landsat-8 imagery (i.e., 30 m spatial resolution) was used for 12 sampled regions around the globe. The number of fire detections ranged from 134 to 8,568 with a false alarm rate ranging between 0% and 1.23%. A full quantitative error analysis, including omission errors, is not yet available due to the limitation of paired reference datasets overlapping in time, which is important for temporal accuracy. However, commission errors found in the initial assessments are deemed minimal, and the newer VIIRS AF product is found suitable for this research.

4.2 Land Cover Product

The European Space Agency's (ESA) Climate Change Initiative (CCI) Global Land Cover (LC) Dataset (i.e., ESA-CCI-LC), detailed in Table 4.1, provides annual land cover maps, from 1992 to 2015, with a 300 m spatial resolution as described in Defourny (2017). The data is compiled from various satellite sources (see Appendix A, Table 2A). The native projection is ellipsoid with a datum of World Geodetic System 1984 (WGS1984). The data is classified using the

United Nations Land Cover Classification System (UN-LCCS). There are 22 classes, and each class is grouped using ten value codes (see Appendix, Figure 2A). This classification system was developed to be compatible with other widely used land cover classification products such as GLC2000 and GlobCover 2005/2009.

Independent validation of ESA-CCI-LC found average 73.4% map accuracy, which is suitable for use in this research (Defourny 2017). This land cover product was selected over the higher resolution Copernicus CORINE Land Cover (CLC) product because the 2018 version of CORINE did not include Turkey. The MODIS global land cover product was also considered since it is used in the MODIS fire product algorithms. However, upon further examination, the product found 96% of the land cover in Tunceli Province to be grassland, and little to no forest was detected. Therefore, the ESA-CCI-LC product was selected for this research.

4.3 SENTINEL SATELLITES

Fire detection and characterization are also carried out with higher resolution imagery such as twin satellites Sentinel-2A and 2B operated by ESA. Sentinel-2A was launched in June 2015 and Sentinel-2B in March 2017. Sentinel-2 products contain 13 spectral bands at three different resolutions (10, 20, 60 m). Data is provided in 100 km^2 tiles of ortho-images (i.e., geometrically corrected images) projected in Universal Transverse Mercator (UTM) with a datum of World Geodetic System 1984 (WGS1984) (European Space Agency 2015). Data is in SENTINEL-SAFE format, including image data in JPEG2000 format, with quality indicators, auxiliary data, and metadata (European Space Agency 2015). The data are corrected for geometry and atmosphere to Level-1C (top-of-atmosphere reflectance) and Level-2A (bottom-of atmosphere reflectance). Level 1C data results from using a digital elevation model (DEM) to project the image in cartographic geometry. Level-2A atmospheric correction provides the true ground reflectance data without interference from atmospheric scattering and also corrections for terrain and cirrus clouds. The products are detailed in Table 4.1.

High-resolution data is preferable for BA mapping, determining severity, and damages. A recent study by Roteta (2019) in sub-Saharan Africa, detected more BA using Sentinel-2 MSI data than MODIS BA data, with higher accuracy compared to global fire products. Furthermore, Roteta (2019) study shows a higher agreement of Sentinel-2 BA and MODIS BA for large patches of BA (> 250 ha) and higher discrepancies for smaller patches of BA (< 25 ha). In regards to the improvement of small fire detection, Roteta (2019) emphasizes the importance of spatial resolution for BA mapping. However, high-resolution data is more commonly used for small areas because use on larger areas can result in noise interference and increases in computing time and processing power. Therefore, Sentinel-2 data is also explored in this research.

TABLE 4.1. DETAILS AND SPECIFICATIONS OF THE REMOTE SENSING PRODUCTS USED

Fire Product	Satellite	Instrument	Years Data Available	Temporal Resolution	Spatial Resolution	File Format	Owner
MODIS BA Product	Terra and Aqua	MODIS	2000/2002 - present	Daily	500 m	Geotiff	NASA
MODIS AF Product	Terra	MODIS	2000 - present	Daily	1 km	shapefile	NASA
MODIS AF Product	Aqua	MODIS	2002 -present	Daily	1 km	shapefile, csv	NASA
VIIRS AF Product	Suomi NPP	VIIRS	2012 -present	Daily	375 m	shapefile	NASA
Sentinel-2	Sentinel-2A	MSI	2015 – present	5 days	10 to 60 m	.SAFE	ESA
Sentinel-2	Sentinel-2B	MSI	2017 - present	5 days	10 to 60 m	.SAFE	ESA
ESA-CCI-LC	Various	Various	1992-2015	Annual	300 m	GeoTIFF	ESA

4.4 CONFLICT DATA

Conflict data are available from the Uppsala Conflict Data Program (UCDP), a well-known, open-source program for providing standardized datasets on conflict events. According to Sundberg and Melander (2013), the conflict data are mined from news sources, governmental and non-governmental organization reports, case studies, historical archives, and other sources. The data are then run through a series of checks for quality and consistency between data sources. Furthermore, UCDP's Georeferenced Event Dataset (GED) organizes conflict data spatially and temporally. Coordinate locations are obtained from sources such as the GEOnet Names Server database (GNS), or maps provided by various non-profit organizations. Each conflict event in this dataset is defined as an instance of organized violence with at least one fatality. Geo-referenced conflict data provide the temporal frequency and spatial distribution of conflict events. Data is provided in WGS84 (World Geodetic System 1984) geodetic datum and distributed in point shapefile file format. Associated data contains important information such as the coordinate location, media source, number of deaths, type of conflict, and actors involved. The conflict data is detailed in Table 4.2.

TABLE 4.2. DETAILS OF THE CONFLICT DATA USED (SUNDBERG AND MELANDER 2013)

Conflict Data	Data Sources	Location Sources	Years (for AOI)	File Format	Owner
UCDP GED	News, reports, archives…	GNS, Google Earth, digital maps…	2003 – 2017	shapefile	UCDP

4.5 DATA RETRIEVAL

All fire products are open source and accessible from the web. The Global Fire Emissions Database (GFED), https://www.globalfiredata.org/, a well-known, open-source database, provides MODIS AF data in a user-friendly CSV format. GFED's analysis tool can be used to subset the data for a specific time and area of interest; however georeferenced data is not available using this tool. This database and the analysis tool is used in phase one of the research (see Section 5.1 for methods).

UCDP conflict data is obtained online (https://www.pcr.uu.se/research/ucdp/ucdp-data/). The GED provides global data of geo-located conflict event in point-shapefile format. Additional conflict data, including, source, location, deaths, etc., are downloaded for the country of interest in XLS format. This data is used in phase one of the research (see Section 5.1 for methods).

The MODIS BA product is downloaded using the USGS Application for Extracting and Exploring Analysis Ready Samples (AppEEARS), https://lpdaacsvc.cr.usgs.gov/appeears/. AppEEARS is a web service that facilitates spatial and temporal subsetting of available geospatial datasets. The data is provided in raster format. MODIS AF and VIIRS AF data are retrieved from NASA's Fire Information for Resource Management System (FIRMS) archive downloader (https://firms.modaps.eosdis.nasa.gov/). FIRMS web service subsets the data for a requested time and area of interest, and the subset data are provided in point-shapefile format. The FTP server and FIRMS web service is used to retrieve data for phase two of the research (see Section 5.2 for methods).

The data 2015 ESA-CCI-LC product is downloaded from the ESA website, http://maps.elie.ucl.ac.be/CCI/viewer/download.php. The data comes in raster format with a user manual and color-scheme layer. This data is used in phase two of the research (see Section 5.2 for methods).

Sentinel surface reflectance products are downloaded from the Copernicus Open Access Hub online interface (https://scihub.copernicus.eu/). Sentinel data tiles are provided in raster format.

This online interface is used to retrieve data for phase three of the research (see Section 5.3 for methods).

5. METHODOLOGY

The study consists of three parts, and each part has its own method with separate results and discussions. Figure 5.1 describes the approach used for each part of the study. Important steps and outcomes in each part of the research are highlighted with colors.

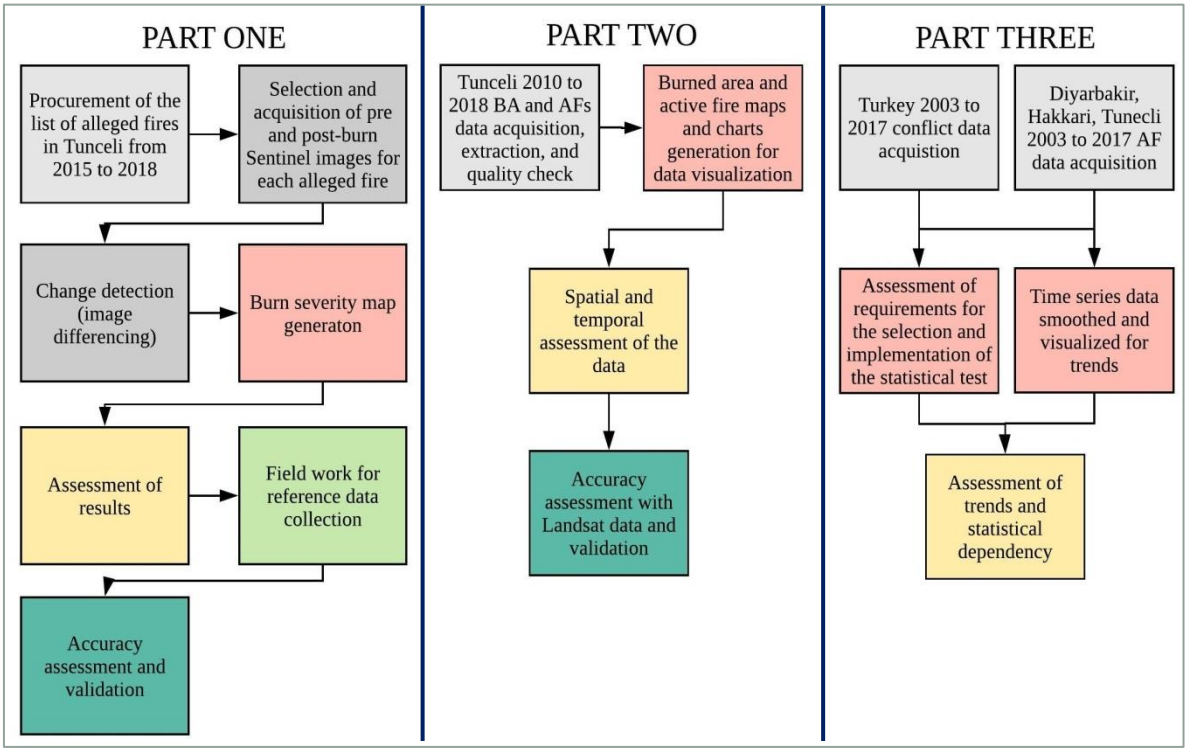

FIGURE 5.1 METHODS USED IN EACH PART (1 TO 3) OF THE RESEARCH

5.1 PART ONE: CHARACTERIZATION OF ALLEGED FIRES IN TUNCELI

The objective of the first part of the thesis is to determine and validate the location of alleged fires described in the claims for Tunceli Province on a local scale and to assess the severity using remote sensing and high resolution imagery. Claims of fires from the years 2015 to 2018 are assessed, which defines the period of the ongoing narratives. High spatial resolution Sentinel products (i.e., 10 m spatial resolution) described in Section 4.3, and change detection techniques described in Section 2.1.1 are used in this part of the thesis to characterize the severity and impact of the fires at a local scale (i.e., < 10 km^2 area). The resulting products are fine scale burned area and fire severity index maps. The final products should be validated with field work data.

5.1.1 *Alleged Fires*

A list of alleged fires was compiled using various media sources and news reports by a researcher at the Center for Middle Eastern Studies at Lund University and provided for this study (Dinc, pers. comm.). Table 5.2 describes the list of alleged fires in Tunceli for years 2015 to 2019.

Table 5.2. Complied list of 13 alleged fires in Tunceli Province from 2015 to 2018 (Dinc, pers. comm.)

Alleged Fires in Tunceli Province from 2015 to 2018			
ID	***Year***	***Location(s)***	***Burn Date***
1	2015	Hozat District	24-Jul
2	2015	Kocakoc Village, Ambar Village	5-Aug
3	2015	Nazimiye District, Bezik Forests	23-Aug
4	2015	Inonu Neighborhood, Pah hamlet	23-Aug
5	2016	Ovacik District, Sultan Baba Mountain	10-Aug
6	2016	Nazimiye District, Dereova Village, Dokuz Kaya Village	28-Aug
7	2017	Kutuderesi, Gokcek Village	09-12 Aug
8	2017	Ovacik District, Ahponos Valley	09-12 Aug
9	2017	Geyiksuyu area	09-12 Aug
10	2017	Sin Village, Bali stream area	09-12 Aug
11	2017	Hozat District, Alibogazi	09-12 Aug
12	2018	Pertek District, Cataksu Village	27-Jul
13	2018	Hozat District, Alibogazi	15-Aug

The precise locations of the alleged fires are not known. The list describes the villages or areas which the fire occurred between. Google Earth digital maps and local knowledge are used to identify the probable area of burn for each alleged fire. If two villages are listed, a line is drawn between them, and the middle point is taken. If three villages/areas are listed, a triangle is drawn, and the center point is taken. Figure 5.2 shows the locations identified for each alleged fire in the list.

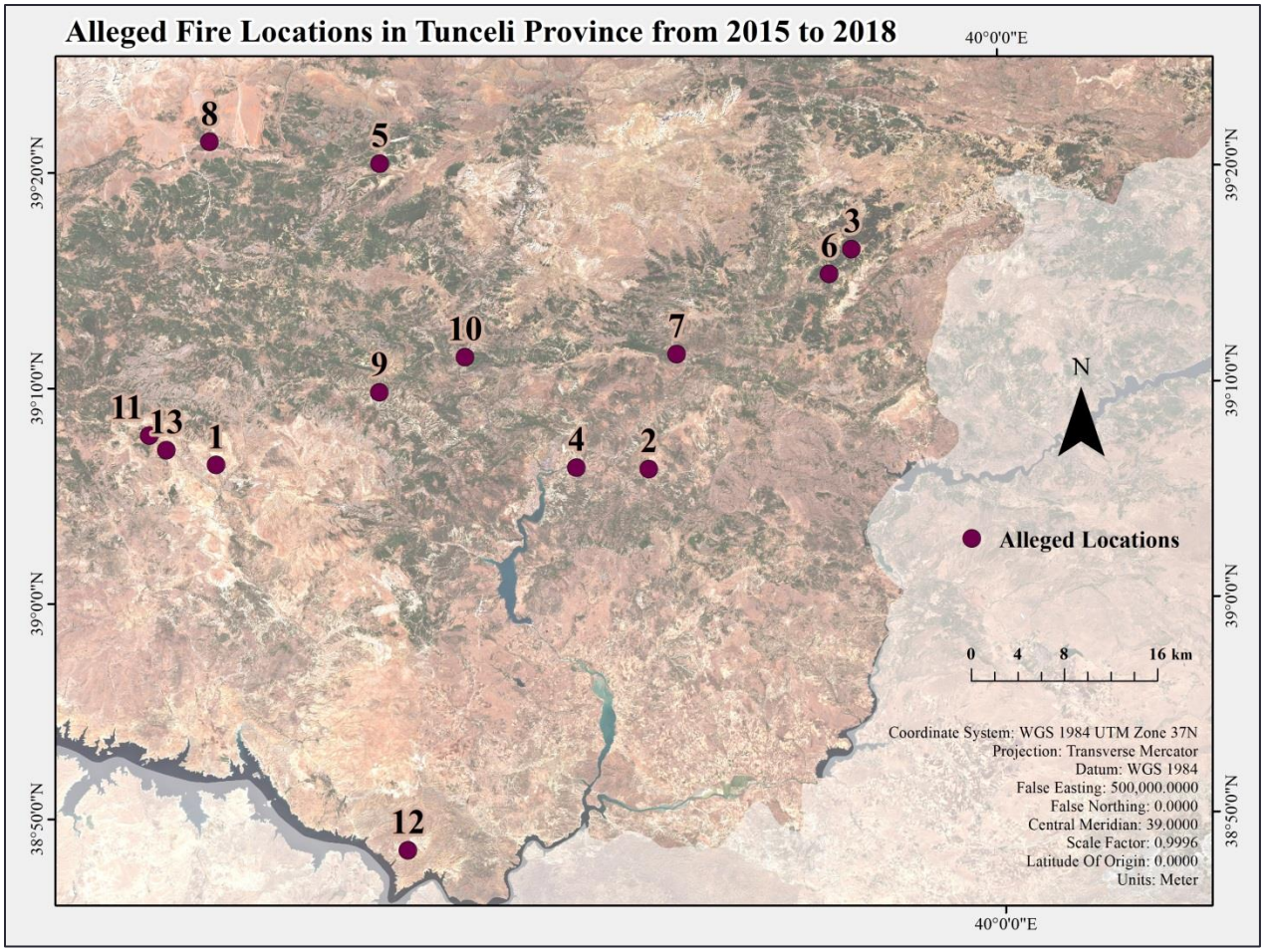

FIGURE 5.2 MAP OF 13 ALLEGED FIRE POINT LOCATIONS FROM 2015 TO 2018 (DINC, PERS. COMM.) IN TUNCELI PROVINCE WITH 2017 SENTINEL-2 TRUE COLOR IMAGERY DOWNLOADED FROM: HTTPS://SCIHUB.COPERNICUS.EU/

5.1.2 SENTINEL DATA SELECTION AND PRE-PROCESSING

Since Sentinel-2A was commissioned October 2015, only one image is available for the 2015 extended dry season, which is inadequate for this study and therefore satellite data from 2015 is not used. Only one Sentinel tile is used (i.e., T37SED) which covers the majority of Tunceli Province. Relatively cloud-free images immediately before and after the alleged burn date are selected for the pre- and post-fire images for the years 2016, 2017, and 2018. All images found were within two weeks before or after the burn date and had less than 40% cloud cover.

For 2016, only Level-1C data is available, so Level-2A corrections (see Section 5.1) are made using Sen2Cor processor. The Sen2Cor processing code was modified to include terrain and cirrus cloud corrections, and all spatial resolutions (i.e., 10, 20, 60 m) are processed for Level-2A (L2A) corrections (see Section 4.3).

5.1.1 Burn Severity Mapping

L2A Sentinel surface reflectance data is further processed using burn index metrics and image differencing techniques found in the Copernicus Research and User Support (2017) training kit for burned area mapping. The method uses the Sentinel Application Platform (SNAP), designed for processing and manipulating Sentinel data.

First, a new band is created containing a cloud mask. Level-2A Sentinel data does contain cloud mask data, but it is time-consuming to apply to all bands of the image using SNAP. For this reason, a conditional statement is used to create the new cloud mask band using the necessary cloud mask data provided (i.e., Sentinel 2 probability-based cloud masks):

if (medium- probability cirrus cloud + high- probability cirrus cloud + thin cirrus cloud) < 255 then 0 else 1

Next, 'GraphBuilder' in SNAP is used to create a set of instructions with operators to batch process the specified images (see Figure 5.3). First, the 'Read' operator reads the selected data, and then these data are resampled to 10 m using bilinear interpolation (i.e., the pixel value is calculated using a linear weighted average of the four nearest pixels). The data is then subsetted using the 'Subset' operator for the bands of interest, which include bands 3, 8, 12, and the previously created cloud mask. Moreover, the Normalized Burn Ratio (NBR) (Eq. 5) is calculated using the 'BandMaths' operator and saved as a new band named 'NBR'.

Eq. 5 $$NBR = (NIR - SWIR) \div (NIR + SWIR) = (B8 - B12) \div (B8 + B12)$$

The newly processed bands are then merged ('BandMerge' operator) so that no band is lost and the results are produced ('Write' operator).

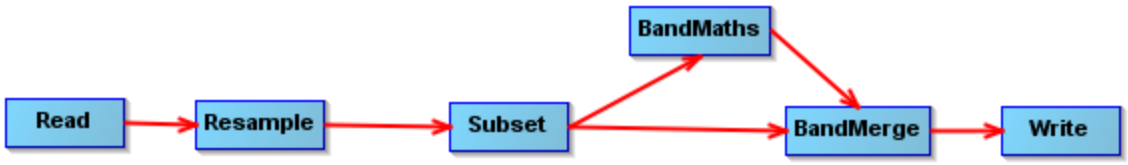

Figure 5.3. Six step Graph built-in 'SNAP' for batch processing selected pre- and post-fire L2A Sentinel-2 images to NBR images (resampled to 10 m^2).

After the writing is complete, the two pre- and post-burn NBR images are merged using the 'Collocation' operator so that the images may be easily differenced. The 'master image' (i.e., pixel values are conserved) is set as the pre-fire image, and the 'slave image' (i.e., pixel values are resampled onto the master grid) is set as the post-fire image.

Since the water bodies can show NBR difference values similar to BA, they need to be masked out along with the clouds. The Normalized Difference Water Index (NDWI) is used to detect water bodies (McFeeters 1996). NDWI maximizes the reflectance of the water in the green band and minimizes the reflectance of water in the NIR band (see Eq. 6).

Eq. 6 $$NDWI = (Green - NIR) \div (Green + NIR) = (B3 - B8) \div (B3 + B8)$$

In SNAP, NDWI is calculated with a conditional statement to determine cloud and water pixels for a combined cloud water mask. This statement is:

if (June's cloud mask > 0 or July's cloud mask > 0 or ((B3 for June – B8 for June)/ (B3 for June + B8 for June))>= 0.0) then 1 else 0

To differentiate BA from other similar looking features such as bare soil and non-vegetated areas, the difference between the pre- and post-burn NBR images is commonly calculated to determine the delta Normalized Burn Ratio (dNBR) as seen in Eq. 7 (Key and Benson 2006).

Eq. 7 $$\mathrm{dNBR} = \mathrm{NBR}_{\mathrm{pre-burn}} - \mathrm{NBR}_{\mathrm{post-burn}}$$

However, the dNBR is an absolute difference which can be problematic in areas with low pre-fire vegetation cover, resulting in a small change between pre-fire and post-fire NBR. In this case, the Relativized Burn Ratio (RBR) (see Eq. 8) is used to understand the relative difference (Parks et al. 2014).

Eq.8

$$\mathrm{RBR} = \mathrm{dNBR}\left(\mathrm{NBR}_{\mathrm{pre-fire}} + 1.001\right) = \mathrm{NBR}_{\mathrm{pre-fire}} - \mathrm{NBR}_{\mathrm{post-fire}}\left(\mathrm{NBR}_{\mathrm{pre-fire}} + 1.001\right)$$

Therefore, a conditional statement is used to calculate the RBR for every pixel not determined as cloud or water. This statement is:

if cloud and water mask == 0 then ((June's NBR – July's NBR)/(June's NBR + 1.001)) else (Not a Number)

In the resulting RBR image, the BAs appear much brighter than the surroundings. To extract the BAs from the surroundings, another conditional statement is used to define a minimum RBR threshold value for BA:

if RBR > 0.10 then RBR else (Not a Number)

The resulting product is the burn severity mask with burn severity (i.e. RBR) values. The burn severity values are interpreted using the USGS burn severity classification system (see Table 5.3) (USGS 2004; Copernicus Research and User Support 2017).

TABLE 5.3. FOUR CLASSES OF BURN SEVERITY RANGING FROM LOW TO HIGH AND DEFINED BY RBR THRESHOLD VALUES BASED OFF USGS BURN SEVERITY CLASSIFICATION SYSTEM (USGS 2004)

Burn Severity Class	RBR Value	Color
Low Severity	0.10 to 0.27	
Moderate-low Severity	0.27 to 0.44	
Moderate-high Severity	0.44 to 0.66	
High Severity	0.66 to 1.30	

Since the alleged fire point locations, in Figure 5.2, are not absolute, a circular buffer is created to search for BA around each point. The buffer size is determined as 10 km, which is relative to the level of uncertainty in the locations provided. Each resulting burn severity mask is visually assessed for BA at least partially within the buffer zone and > 500 pixels (i.e., > 5 ha). The criterion was determined by the local community who recognized significant forest fires as > 5 ha. Pixels that are apparently misclassified as BA by the change detection are disregarded (e.g., sunglint, etc.). Also, as a general guideline, BA pixels are grouped or close together, with no more than 3 km of unburned pixels between the outermost burned pixels. The pixel group is then extracted from the rest of the burn severity mask and considered one combined fire. The total area burned, and the levels of severity are measured for each fire detected.

5.1.2 FIELD WORK

Field work aims to validate the fires detected and verify that each fire is correctly classified by the methods. Positional accuracy is not as important here, rather the correctness of the thematic classification (i.e., the burned areas detected). Field work will not attempt to validate the burn severity classification, but simply focuses on the presence or absence of burned area at each location. Due to time constraints only one or two sample points for each of the eight fire locations detected are visited to search for evidence of burning. If the total burned area is > 1 km^2, two well-distributed sampling points in the detection area are visited. If the total burned area is < 1 km^2, then only one sampling point is visited, ideally in the middle of the detection area.

At each sample point a homogenous area of approximately 200 m^2 is assessed for evidence of burning. Evidence of burning includes scorch marks, presence of char, and apparent damage to

the vegetation (USDI National Park Service 2003). If evidence of burning is observed, then, the fire detection is considered to be correct. For fires > 1 km^2 evidence of burning should be found at both sample locations. If evidence of burning is only found at one sample location, then the fire detection is considered only partially correct. Tentative sample sites are planned prior to the field visit but may change depending on site accessibility. During the site visit, accurate geolocated points are obtained using an available Global Positioning System (GPS). Detailed field observation sheets are filled and photographs are taken at each site (see Appendix B). Any relevant information about the fires is noted down (see Appendix A, Table 11A). Finally, the field data will be compared with the burn severity maps and will together either be used to support or negate the claims of the fires found in Table 5.2.

5.2 Part Two: Analysis of Tunceli Fires

The second part aims to extract, assess, and validate active fire (AF) and burned area (BA) data from the most advanced remotely sensed fire data products for the case study area of Tunceli Province. In this part, the fires are assessed from 2010 to 2018 for each extended dry season (i.e., May to October) using MODIS BA, MODIS AF, and VIIRS AF products outlined in Table 4.1. The selected period accounts for changes in violent conflict in the PKK-Turkish War and incorporates the recent development of narratives starting in 2015 (see Sections 1.1 and 1.2). BA and AF data patterns are assessed with these changes. An accuracy assessment is carried out for both MODIS and VIIRS products to understand the usability of the data.

5.2.1 Data Extraction and Quality Check

All data is spatially and temporally subsetted to Tunceli Province, beginning May to the end of October, totaling of 256 days for each extended dry season. MODIS products are available for the full assessment period, however VIIRS products are only available starting 2012. For visualization, all the data is re-projected to Transverse Mercator with a geodetic datum of World Geodetic System 1984 Zone 37N (i.e., WGS 84/UTM Zone 37N (EPSG: 32637)) which accommodates most of Eastern Turkey and is compatible with Google Earth for sharing purposes.

The MODIS BA subset data includes 54 monthly burn date raster layers for the requested periods. The data is reclassified in ArcMap to temporally aggregate the burned pixels by month and year. MODIS and VIIRS AF shapefile attributes contain information about the acquisition date and time. This information is used to count and assess the number of yearly and monthly AF detections.

The MODIS BA quality assurance data, provided by the algorithm, indicated that only 0.02% of data had a ‘false valid data flag’, meaning that there was insufficient valid data for the grid cell

to be processed in the time series. This means that 99.98% of all pixels in the times series contained valid data. Additionally, it is good to note that only 0.01% of the pixels first flagged as burned by the algorithm, had special circumstances for later being classified as unburned in the final product, such as large time distance between observations, or burn date of the pixel was too close to the limit of times series to be properly assessed.

MODIS AF product confidence level ranges from 0 to 100% and VIIRS ranges from low, nominal, and high levels of confidence. The confidence of detection for both VIIRS and MODIS products is detailed in Appendix A, Table 5A and 6A. For the data used, MODIS AF product has a 60% confidence level, corresponding to moderate to high levels of confidence in detection and 80% of VIIRS data has a high level of confidence.

Additionally, the ESA-CCI-LC product is used to extract the type of land cover burned. This is done by cross-tabulating BA and the land cover dataset to determine the land cover type and area burned. The resulting land cover types are re-grouped into three general classes, natural vegetation, cropland, and bare land.

5.2.2 Accuracy Assessment of Fire Products

Accuracy assessments of MODIS BA, MODIS AF, and VIIRS AF products are done using higher-resolution (i.e., 30 m) Landsat data. Assessing the accuracy of AF and BA data with higher-resolution imagery, such as Landsat, is a common approach, especially when validation on the ground is difficult because of limited accessibility, vegetation regrowth, and/or land use changes over time (Schroeder et al. 2014; Fornacca et al. 2017; Giglio et al. 2018b). Landsat images immediately before and after the burn date are ideally used to visually assess for signs of fire. However this is dependent on image availability, considering Landsat's 16 day revisit time, and cloud interference. Typically usable images are found within day(s) to week(s) before and after the burn date. Landsat is selected over higher resolution Sentinel data (i.e., 10 to 20 m) for its complete temporal coverage for the years of interest.

Landsat scenes are downloaded online using USGS Earth Explorer (https://earthexplorer.usgs.gov/). They are organized using the Worldwide Reference System (WRS), and each scene is identified with a path, row number. For Tunceli path 173 and row 33 is used. The scenes are processed to the highest-quality, Level 1 'standard terrain correction or L1TP', which includes radiometric and relief displacement corrections.

The Landsat images are visualized using the shortwave infrared (SWIR), near-infrared (NIR) and red (R) bands. This combination clearly shows the burn scars. Burn scars are also apparent in natural color (i.e., red, green, blue (RGB)), but they are sometimes more difficult to visualize compared to the longer wavelengths (i.e., SWIR and NIR).

The accuracy assessment uses a simple two-step approach, described in Congalton and Green (2009). Initially, one season of fire data is selected; typically a year with relatively more fires. Since fires are infrequent, in this case, less than 1% across the entire region, stratification to prioritize the fire detections is necessary (Congalton and Green 2009).

First, the pixels within each product are divided into two populations or strata. One population consists of vegetated area where no fires are detected (i.e., unchanged areas) and the second where fires are detected by the product (i.e., changed areas). Then 50 pixels or 'samples' are randomly selected from each population for each product (Lillesand and Kiefer 1994). Second, the validation is performed; where the maps are treated as a binary scheme of change/no change or burned/unburned. If signs of burning are partially within the fire pixel and within a month of the product's burn date, the product is considered to detect the fire correctly. After validation, a final burned/unburned contingency matrix is created to determine the error of omission, the error of commission, producer's accuracy, user's accuracy, overall accuracy, and the kappa coefficient (Olofsson et al. 2014). The kappa coefficient measures the observed agreement between the reference and classification data and adjusts for the amount of agreement that could be expected due to chance alone (e.g., based on the resolution of the image or total rows and columns) (Congalton and Green 2009). The thresholds, found in Table 5.1, are purposed by Landis and Koch (1977) and are used to interpret the kappa values.

TABLE 5.1. KAPPA RANGES AND AGREEABILITY (LANDIS AND KOCH 1977)

Kappa Range	Agreement
> 0.80	Strong agreement
0.40 to 0.80	Moderate agreement
< 0.40	Poor agreement

5.3 PART THREE: DATA VISUALIZATION AND STATISTICAL ANALYSIS OF FIRE AND CONFLICT EVENTS

Part three aims to determine the accounts of fires for three recognized conflict areas at the provincial scale and to evaluate the accounts within the context of conflict and political stability, at the national scale, presented in Sections 1.1 and 1.2. The areas of interest for the accounts of fires include Tunceli, Diyarbakir, and Hakkari provinces (see Figure 3.1). Numbers of fires per year (i.e., MODIS AF counts) are obtained using the GFED (see Section 4.5). Reports of armed conflict per year are obtained from the UCDP (see Section 4.4). This data will be used to observe

conflict dynamics over time and will quantitatively represent the historical political context described in Section 1.1.1 (see Figure 1.1).

The time series data is visualized using the moving average smoothing technique. This technique removes fine scale variations allowing patterns in the data to be visualized more clearly over the time period of interest. The moving average is calculated by replacing each successive observation in a time series by the mean of the term of the sequence (Burt et al. 2009). The term of the sequence is noted as t. For example, if t = 5 then, the first five data values (i.e., x_1, x_2… x_5) are averaged to produce the first mean of the moving average at the location of the 5^{th} observation. The mean of the 6^{th} observation in the time series is calculated used the next five data values (i.e., x_2, $x_{3...}$ x_6) and so on. This smoothing technique replaces the original time series with a new series of "moving" means (Burt et al. 2009). The resulting smoothed data will be used to assess trends to understand if fires in each area of interest are increasing after the year 2015 in correspondence to the ongoing narratives.

Furthermore, statistical testing is carried out to understand the relationship between the fire and conflict data. While the datasets are compared, there is no way to understand if one caused the other without ground truth data and the identification of the ignition source. Therefore, caution must be used to avoid any implication of causation while interpreting the results of the statistical analysis.

To note, Turkey's conflict data is only used to quantitatively represent fluctuations in the ongoing conflict at the national-scale. In this way, the actual distance between the conflict events and the fire events are not of interest and effects of spatial autocorrelation (i.e., the correlation of a variable with itself over space) are avoided. Additionally, temporal autocorrelation (i.e. the linear association of a single variable over time) of both datasets is assumed to be zero for simplicity.

5.3.1 Statistical Analysis

Statistical analysis and testing is done to assess the relationship between fire occurrences and conflict for each area of interest (i.e., Tunceli, Diyarbakir, Hakkari) from 2003 to 2017. Here the fire count data and the conflict data are treated as the dependent and the independent, continuous variables respectively. The analysis between these two variables takes place in three steps: 1) each dataset is tested for a normal (i.e., parametric) or non-normal (i.e., non-parametric) distribution (e.g., using kurtosis and skewness values and Shapiro-Wilk) 2) data is assessed for a linear, monotonic, or non-monotonic relationship between the two variables (e.g., using scatterplots and correlation coefficients) 3) based on the results of the first two steps a statistical technique is selected to find the relationship between the two datasets (e.g., Pearson's correlation

test, Spearman rank correlation test…). These preliminary steps are presented in the following text and the results from the determined statistical analysis are presented in Section 6.

1) Test for Normality: Parametric vs. Non-parametric Determination

The first indication of distribution is shown by the calculated skewness and kurtosis values for each dataset. The symmetry and peak(s) of the distribution are respectively described by the skewness and kurtosis values (Pallant 2005). A perfectly normal, bell-shaped distribution, would have kurtosis and skewness values at 0 (Pallant 2005). However, while the closer the kurtosis and skewness values are to 0, the better, a general range of –2 to 2 is accepted as normally distributed (George and Mallery 2010).

Two of the four datasets both had kurtosis or skewness values outside of the accepted threshold of -2 to 2 (see Appendix, Table 11A), indicating non-normal distributions. Therefore, the data was further tested for normality using the Shapiro-Wilk test (Shapiro and Wilk 1965). For the Shapiro-Wilk test, the calculated p-value (i.e., statistical probability) was compared with a 95% confidence level, $\alpha = 0.05$ (i.e., level of significance) (Fisher 1934). A p-value > α determines a normal distribution and a p-value < α determines a non-normal distribution. Since two of the four datasets are found to have a non-normal distribution; a non-parametric statistical test, such as Spearman-Rank correlation test, should be selected and applied to all the datasets for consistency. The full results of the Shapiro-Wilk test are found in Appendix A, Table 12A.

2) Monotonic, or Non-monotonic Determination

However, before the Spearman-Rank test is applied the data is assessed for the presence of a monotonic relationship, which is requirement by the test. The first visual assessment of the scatterplots shows the possibility of a monotonic relationship between the fire data for each area of interest and the conflict data (see Appendix A, Figure 2A). To be certain, the spearman correlation coefficients (r_s) are calculated and a hypothesis test is applied. Like Pearson's correlation coefficient, Spearman's correlation coefficient falls between – 1 and 1. The sign of the coefficient represents the direction of the relationship and the value represents the strength of the relationship. The null hypothesis, H0, states that there is no monotonic correlation between the fire and conflict datasets (i.e., $r_s = 0$). The alternative hypothesis, H1, states that there is a monotonic correlation between the two populations (i.e., $r_s \neq 0$). Each of the three areas of interest observed $r_s \neq 0$, indicating a monotonic relationship. This test satisfies the assumption of the presence of a monotonic relationship; therefore, the non-parametric Spearman-Rank correlation test is selected and applied to each area of interest for consistency and comparability.

3) Statistical Hypothesis Test Determination: Spearman-Rank

The Spearman-Rank statistical test is selected to understand the relationship between the fire and conflict datasets using hypothesis and significance testing (Spearman 1904). The test is rank-

based and measures the correlation based off the average ranks. The null (H0) and the alternative hypothesis (H1) are defined as follows: H0: there is no statistically significant relationship between the fire and conflict datasets, and H1: there is a statistically significant relationship between the fire and conflict datasets.

First, both conflict and fire datasets for the area of interest are separately ranked in ascending order. If the ranks are tied, the tied ranks are averaged. Next, the Spearman's correlation coefficients (r_s) are calculated for each area of interest (completed in pervious step). The coefficient, r_s, is calculated using Eq. 3 (Spearman 1904).

Eq.3
$$r_s = 1 - \frac{6\sum_{i=1}^{n} d_i^2}{n^3 - n}$$

n is the sample size, d_i^2 is the squared difference between the ranks, and i is the observation within the dataset.

The resulting r_s is used to find the t-value, distributed as the Student's t distribution (i.e. a two-tailed continuous probability distribution for small sample datasets), with $n - 2$ degrees of freedom using Eq. 4. The confidence level is determined to be 95% with $\alpha = 0.05$ (Fisher 1934).

Eq.3
$$t = r_s \sqrt{\frac{(n-2)}{(1-{r_s}^2)}}$$

Then the p-value is found using the absolute value of t and the degrees of freedom. Finally, the resulting p-value is compared to $\alpha = 0.05$ to determine if the null hypothesis is rejected. If the p-value $\geq \alpha$, the null hypothesis is rejected, and if the p-value $< \alpha$, the null hypothesis is not rejected.

6. RESULTS

The results from parts one to three described in the methodology (see Section 5) are provided in this section. Results from each part are presented in individual sections.

6.1 PART ONE RESULTS

The change detection technique implemented in part one (see Section 5.1) was used to determine the probable locations and severities of the alleged fires from 2016 to 2018.

Primarily low to moderately-low severity fires are detected for each alleged fire listed in Table 5.2 from 2016 to 2018 using the method described in Section 5.3. Burn scars, of at least 5 ha, are detected within the 10 km circular buffer zone, for all nine alleged locations from 2016 to 2018. Figure 6.9 shows the locations of the detected fires within or touching the 10 km circular buffer centering on the alleged fire location (Dinc, pers. comm.).

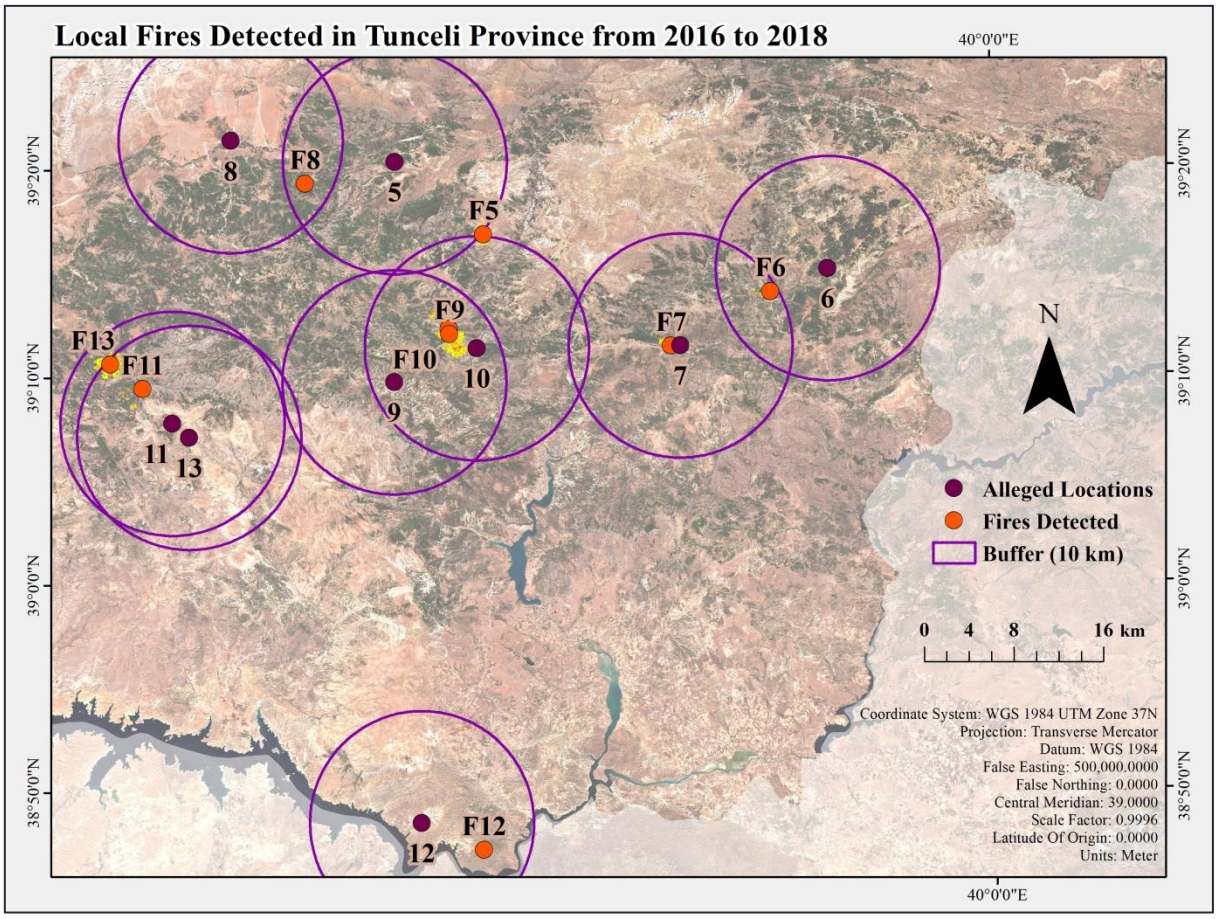

FIGURE 6.9 LOCATIONS OF THE 13 FIRES DETECTED IN RED (ID = F5 TO F13) WITH THE ALLEGED LOCATIONS (DINC, PERS. COMM.) IN YELLOW (ID = #5 TO #13) CENTERING CIRCULAR 10 KM BUFFERS (PURPLE) USED IN THE BURN SCAR DETECTION. THE 2017 SENTINEL-2 TRUE COLOR IMAGERY WAS DOWNLOADED FROM: HTTPS://SCIHUB.COPERNICUS.EU/

The nine fires totaled 12.05 km^2 of BA. Of this 77% are low severity, 20% are moderate-low severity, 3% are moderate-high severity, and << 1% are high severity burns.

The largest fire is depicted in Figure 6.10 (F9, F10) and incorporates 4.78 km^2 of BA. This fire occurred in 2017 just west of Munzur Valley National Park near Karsilar Village. There are two corresponding claims referring to a fire near Geyiksuyu (Figure 6.10 (F9)) and Sin Village (Figure 6.10 (F10)) areas which are less than 10 km away from each other, leading to overlap in

detection areas. It is possible these two claims refer to the same fire since no other large fires were detected in the areas. Approximately 75% of this fire is detected as low, 23% is detected as moderate- low, 2% is detected as moderately-high, and << 1% is detected as high severity burns (see Figure 6.10 (F9; F10)). Another larger fire, shown in Figure 6.10 (F13), is detected near Hozat District in 2018, burning 3.28 km^2 with 89% low, 10% moderately-low, and 1% moderately-high to high severity burns. Additionally, a more severe fire of 1.79 km^2 is found near Ovacik District in 2016 (Figure 6.10 (F5)) with 50% low, 38% moderately-low, 12% moderately-high to high severity burns. The other five fires are all less than 1 km^2 with burn severities ranging from low to moderately-high.

F11 and F12 in Figure 6.10 show BA as a group of discontinuous pixels; this is likely due to the insensitivity of the algorithm to the variations in the background (i.e., soil color, terrain, vegetation type…). Furthermore, the ESA-CCI-LC product was used to visually check land cover type, since field data could not be obtained. All nine fires correspond to natural vegetation classes (e.g., value ID = 100, mosaic tree and shrub > 50%/ herbaceous cover < 50%). See Appendix A, Table 3A for detailed information on the burn severity of each fire detected.

Unfortunately, due to unforeseen restrictions/limitations in access, the maps of the alleged fires were not validated. Additionally, due to time constraints, field work was carried out in April 2019, which is early spring in Tunceli, so trees are typically just starting to bud, and the lack of leaves made assessing fire damage from afar difficult. Despite the unfortunate circumstances, some information was obtained from casual discussions with locals about the fires. While no formal interviews or assessments were made, insight about the fires and the narratives surrounding them was gained.

Discussions with locals were limited to eight anonymous people, because of ethical considerations for the research. It seems there is a common consensus that the Turkish state starts the fires in the area. A few noticed that the fires started to increase in 2015 after the solution process ended. They claim they are not aware of other reasons for the fires because the forests are primarily oak, which is difficult to burn, and is the reason many fires go out naturally. A local said, ‘They are doing this even when there are no terrorists here, they are doing it to terrorize, they are destroying nature to make us leave this place.’

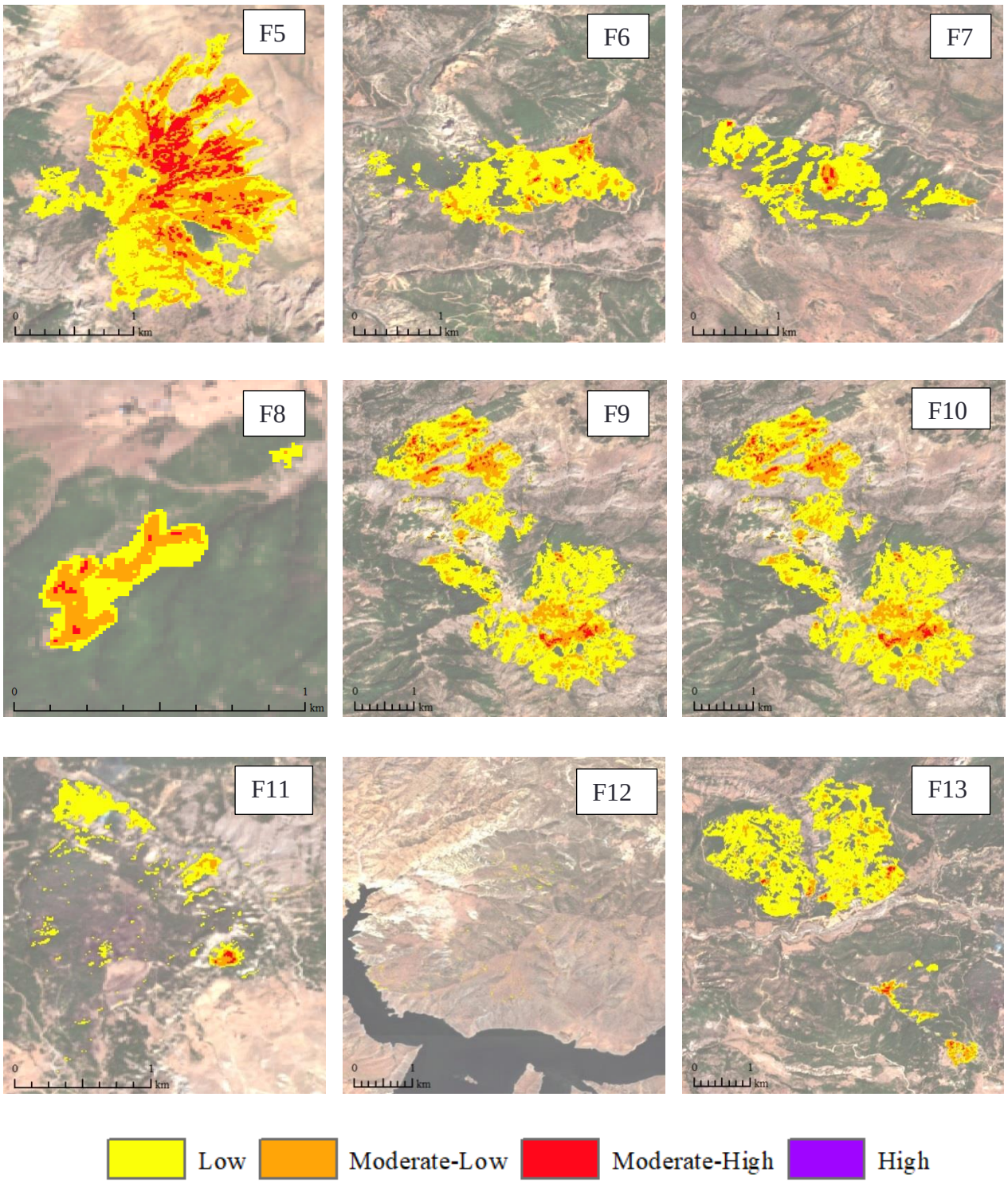

FIGURE 6.10 BURN SEVERITY FIGURES FOR THE LOCAL FIRES DETECTED (ID = F5 TO F13) IN TUNCELI FROM 2016 TO 2018

6.2 PART TWO RESULTS

MODIS and VIIRS fire products were used to determine the accounts of fires in Tunceli Province, from 2010 to 2018, and the accuracy was assessed. The burned area (BA) and active fire (AF) data for Tunceli, from 2010 to 2018, extended dry seasons (i.e., May to October), all show increases in detection after the year 2014. The results are presented in Figures 6.3 to 6.5. Charts show the trend of fire data from 2010 for MODIS products (Figure 6.3 and 6.4) and from 2012 for the VIIRS product (Figure 6.5). Maps of Tunceli show the locations of the detected fires for each product with the 2015 ESA-CCI-LC product (see Appendix A, Figure 1A for the legend). Since the maps show all fire detections over the nine years, some pixels or points overlap, especially in areas of higher fire activity. All products found overall accuracy of > 90%.

6.2.1 YEARLY DRY SEASON ACCOUNTS

From 2010 to 2018, the total BA during the extended dry season in Tunceli is 22.32 km^2. Figure 6.3 illustrates the total BA for all nine years. The largest amount of total BA from all nine dry seasons is found in 2016 at 5.58 km^2. No fires are detected in the 2010 and 2014 dry seasons. 2018 saw the second highest BA total since 2016, at 4.72 km^2. A general increase in BA after the year 2015 is observed.

MODIS and VIIRS AF products detected 106 and 692 fires respectively for all nine dry seasons. For both products, fire count is highest in 2017, with 38 and 233 fires detected for MODIS and VIIRS products respectively (see Figure 6.4 and 6.5). Fire counts for both products show an increase in the number of fires after the year 2015.

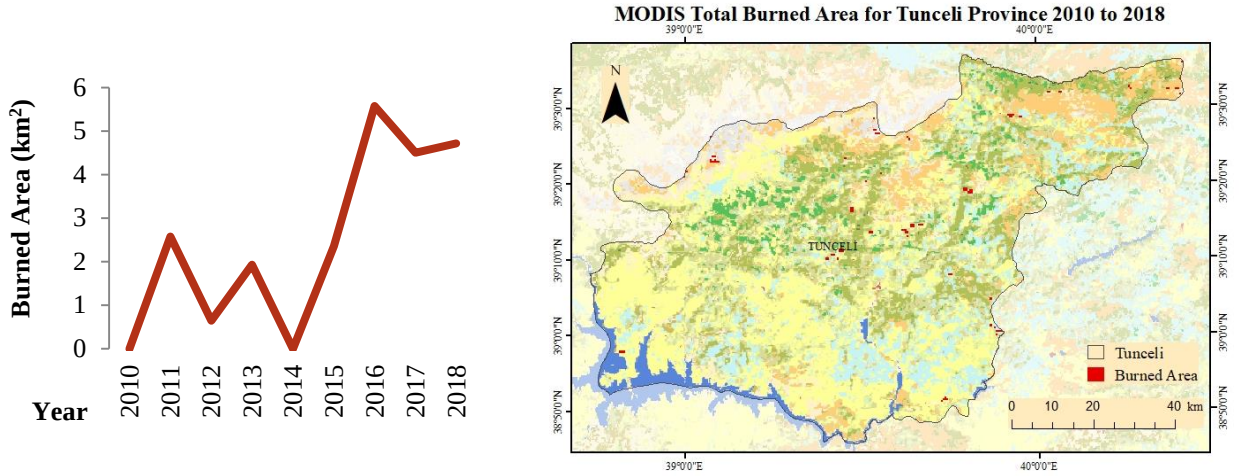

FIGURE 6.3 MODIS BA TOTALS FROM 2010 TO 2018 EXTENDED DRY SEASONS IN TUNCELI

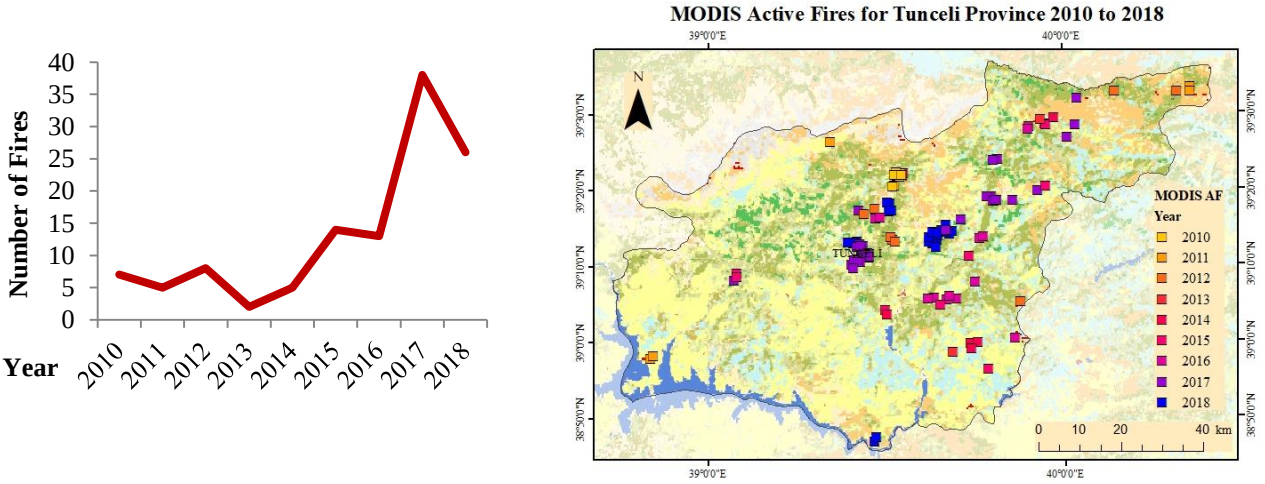

FIGURE 6.4 MODIS AF COUNTS FROM 2010 TO 2018 EXTENDED DRY SEASONS IN TUNCELI

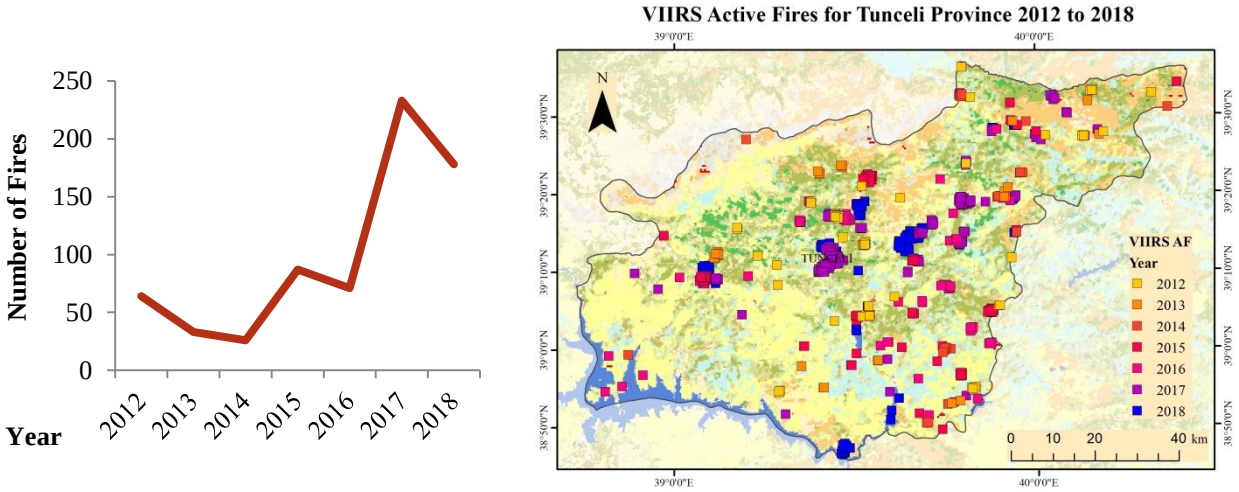

FIGURE 6.5 VIIRS AF COUNTS FROM 2012 TO 2018 EXTENDED DRY SEASONS IN TUNCELI

6.2.2 *Monthly Dry Season Accounts*

The BA data is analyzed monthly for each dry season as described in Figures 6.6. September had the largest relative amount of BA summing to 9.7 km^2, with most of the BA observed after 2014. The largest total BA for any month is September with 2.79 km^2 (for both 2017 and 2018). 2015 is the only year to observe BA every month except October during the dry season.

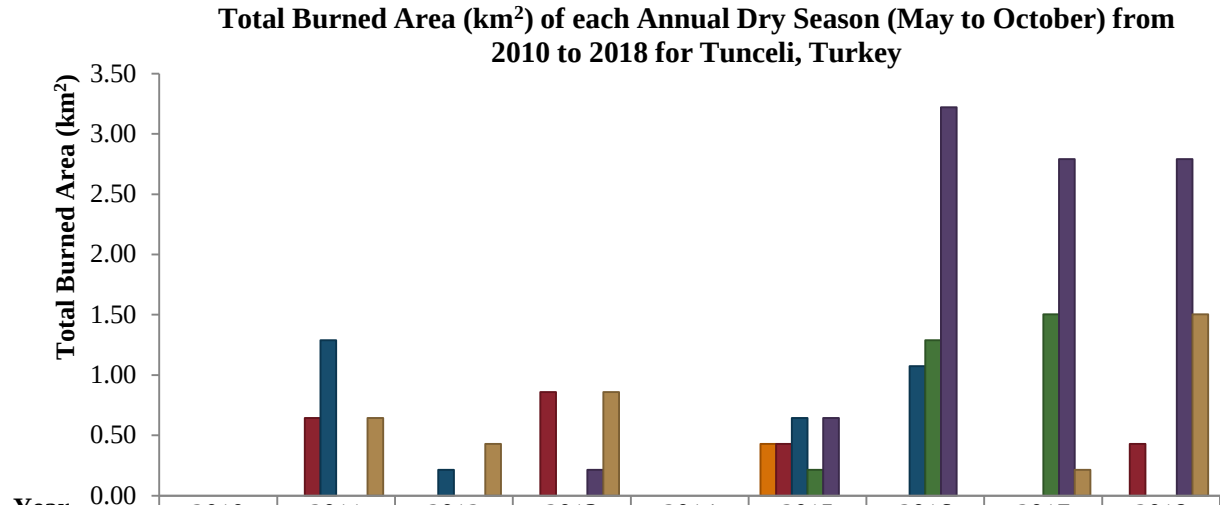

Year	2010	2011	2012	2013	2014	2015	2016	2017	2018
May	0.00	0.00	0.00	0.00	0.00	0.43	0.00	0.00	0.00
June	0.00	0.64	0.00	0.86	0.00	0.43	0.00	0.00	0.43
July	0.00	1.29	0.21	0.00	0.00	0.64	1.07	0.00	0.00
August	0.00	0.00	0.00	0.00	0.00	0.21	1.29	1.50	0.00
September	0.00	0.00	0.00	0.21	0.00	0.64	3.22	2.79	2.79
October	0.00	0.64	0.43	0.86	0.00	0.00	0.00	0.21	1.50

FIGURE 6.6 MONTHLY MODIS BA TRENDS FOR TUNCELI FROM 2010 TO 2018

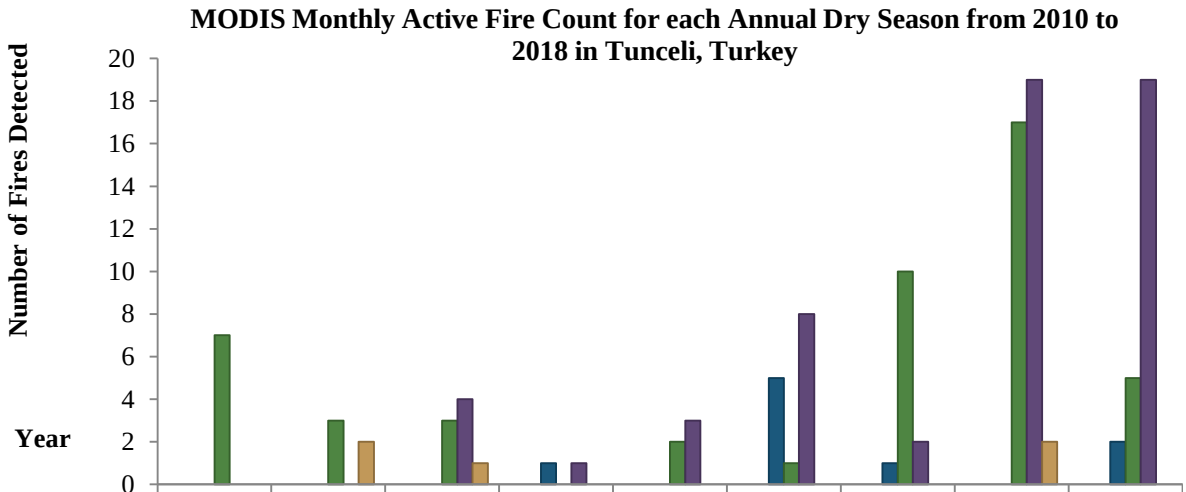

	2010	2011	2012	2013	2014	2015	2016	2017	2018
May	0	0	0	0	0	0	0	0	0
June	0	0	0	0	0	0	0	0	0
July	0	0	0	1	0	5	1	0	2
August	7	3	3	0	2	1	10	17	5
September	0	0	4	1	3	8	2	19	19
October	0	2	1	0	0	0	0	2	0

FIGURE 6.7 MONTHLY MODIS AF DATA FOR TUNCELI FROM 2010 TO 2018

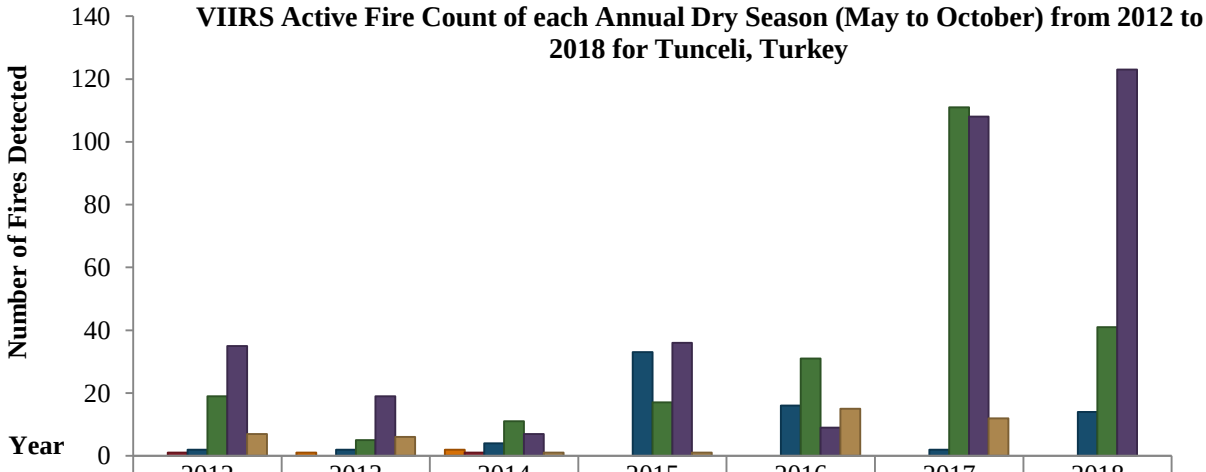

	2012	2013	2014	2015	2016	2017	2018
May	0	1	2	0	0	0	0
June	1	0	1	0	0	0	0
July	2	2	4	33	16	2	14
August	19	5	11	17	31	111	41
September	35	19	7	36	9	108	123
October	7	6	1	1	15	12	0

FIGURE 6.8 MONTHLY VIIRS AF DATA FOR TUNCELI FROM 2012 TO 2018

The MODIS and VIIRS AF data is also analyzed monthly as shown in Figure 6.7 and 6.8 respectively. Both MODIS and VIIRS AF products show higher fire counts in August and September each season. May had the lowest fire count of both the products. The largest amount of fires detected by both products for any month is in September 2018, where VIIRS detected 123 fires and MODIS detected 19 fires. Refer to Appendix A, Table 7A to 9A for detailed AF and BA data tables.

6.2.3 Land Cover Type Burned

The results of the land cover extraction found that natural vegetation cover accounts for 48% of the BA (see Table 6.2). The type of vegetation burned from most BA to least BA is as follows: grassland (4.50 km^2), mixed of trees, shrubs, and herbaceous (3.65 km^2), mix of tree and shrub (1.50 km^2), and sparse vegetation of mixed trees, shrubs and herbaceous (1.07 km^2) (see Appendix A Table 10A). Additionally, cropland accounts for 34%, and bare land accounts for 18% of the total burned area (see Table 6.2).

TABLE 6.2 THE TOTAL AMOUNT OF LAND COVER BURNED PER LAND COVER GROUP (I.E., NATURAL VEGETATION, CROPLAND, BARE; MODIFIED FROM ESA-CCI-LC) FOR ALL EXTENDED DRY SEASONS (I.E., 2010 TO 2018)

Type	Area Burned (km^2)	%
Natural Vegetation	10.73	48%
Cropland	7.51	34%
Bare	4.08	18%
Total	22.32	100%

6.2.4 Accuracy Assessment of Fire Products

The year 2017 is selected for the accuracy assessment since it had the most fires during the extended dry season. Table 6.3 describes the sampling breakdown. VIIRS AF had over 50 fires; however, both MODIS AF and BA had less than 50, so all available fire pixels are sampled for those products.

TABLE 6.3 SAMPLING STRATIFICATION FOR THE 2017 ACCURACY ASSESSMENT OF THE FIRE PRODUCTS (I.E., VIIRS AF, MODIS AF, AND MODIS BA)

Sampling Breakdown of Strata		
Strata	**% of Total Samples**	**Number of Samples**
VIIRS AF	21%	50
MODIS AF	100%	38
MODIS BA	100%	21
Unburned (Vegetated Area)	0.10%	50

The overall accuracy and kappa coefficients for all three products are high (i.e.,> 90% or > 0.80). VIIRS AF has the lowest overall accuracy and kappa, and MODIS AF has the highest overall accuracy and kappa. According to the Landis and Koch (1977) purposed thresholds for kappa interpretation (see Table 5.1); all kappa values show strong agreement between the products and the reference data. The results of the accuracy assessment are presented in Table 6.5 to 6.7.

TABLE 6.5. 2017 VIIRS AF ACCURACY MATRIX AND ASSESSMENT RESULTS

		Reference Image				
		BA	*Unburned*	*Total*	*Error of Commission*	*User's Accuracy*
VIIRS AF	*BA*	43	0	43	0%	100%
	Unburned	7	50	57	12.3%	87.7%
	Total	50	50	100		
	Error of Omission	14%	0%			
	Producer's Accuracy	86%	100%			**Total: 93%**
						Kappa: 0.86

TABLE 6.6. 2017 MODIS AF ACCURACY MATRIX AND ASSESSMENT RESULTS

		Reference Image				
		BA	*Unburned*	*Total*	*Error of Commission*	*User's Accuracy*
MODIS AF	*BA*	36	1	37	2.7%	97.3%
	Unburned	2	37	39	5.1%	94.9%
	Total	38	38	76		
	Error of Omission	5.3%	2.6%			
	Producer's Accuracy	94.7%	97.4%			**Total: 96.1%**
						Kappa: 0.92

TABLE 6.7. 2017 MODIS BA ACCURACY MATRIX AND ASSESSMENT RESULTS

		Reference Image				
		BA	*Unburned*	*Total*	*Error of Commission*	*User's Accuracy*
MODIS BA	*BA*	19	0	19	0%	100%
	Unburned	2	21	23	8.7%	91.3%
	Total	21	21	42		
	Error of Omission	9.5%	0%			
	Producer's Accuracy	90.5%	100%			**Total: 95.2%**
						Kappa: 0.90

6.3 Part Three Results

In part three, conflict and fire data is evaluated within the sociopolitical context, visually assessed for patterns, and compared using statistical analysis. The results show that the conflict data is reflective of the political context provided in the introduction, the smoothed fire data increases after the year 2014, and statistically significant correlations between the conflict and fire datasets are found across all areas of interest.

6.3.1 Data Visualization

According to the UCDP, 94% of conflicts in Turkey, from 2003 to 2017, are between Turkey and Kurdish insurgent groups. The primary opposing sides are the Turkish government and the PKK. The number of conflicts is consistent with the historical political context described in Section 1.1. Figure 6.1 shows the number of conflicts reported in Turkey, from 2003 to 2017, with the historical timeline (modified from Figure 1.1 in Section 1.1). The conflict data, shown in black, fits well with the historical political context consisting of years with declined conflict in blue and years with increased conflict in red. This indicates that the UCDP dataset for Turkey for the given time period well-represents the fluctuations in political stability and conflict in the ongoing PKK-Turkish war.

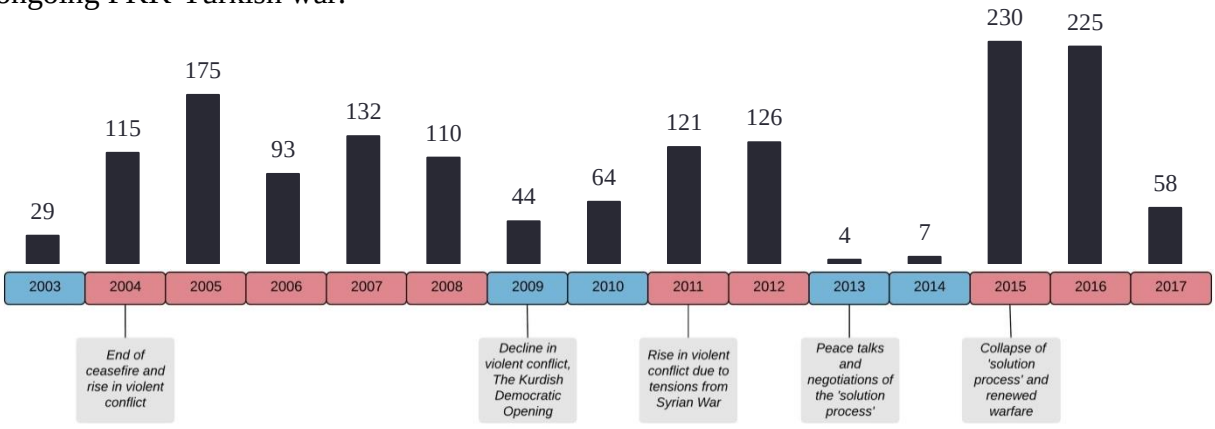

Figure 6.1 Historical timeline of political events (modified from Figure 1.1 in Section 1.1) overlaid by the UCDP conflict data for Turkey from 2003 to 2017. Red years indicate increased conflict and blue years indicate decreased conflict.

One noticeable trend consistent in Turkey's conflict data is the large decrease in conflict in 2013, marking the start of the peace process, followed by the large increase in conflict in 2015, marking the collapse of the peace process (see Figures 6.1). This same pattern is observed in the fire data for Tunceli (see Figure 6.2 A). Tunceli, Hakkari, and Diyarbakir provinces all show a positive increase in number of fires after the year 2015 (see Figure 6.2 A, B, C). However, the increasing trends is more mild for Diyarbakir Province (see Figure 6.2 C). The smoothed conflict data for Turkey is included in Figure 6.2 for to aid in visual comparison (see. Figure 6.2 D).

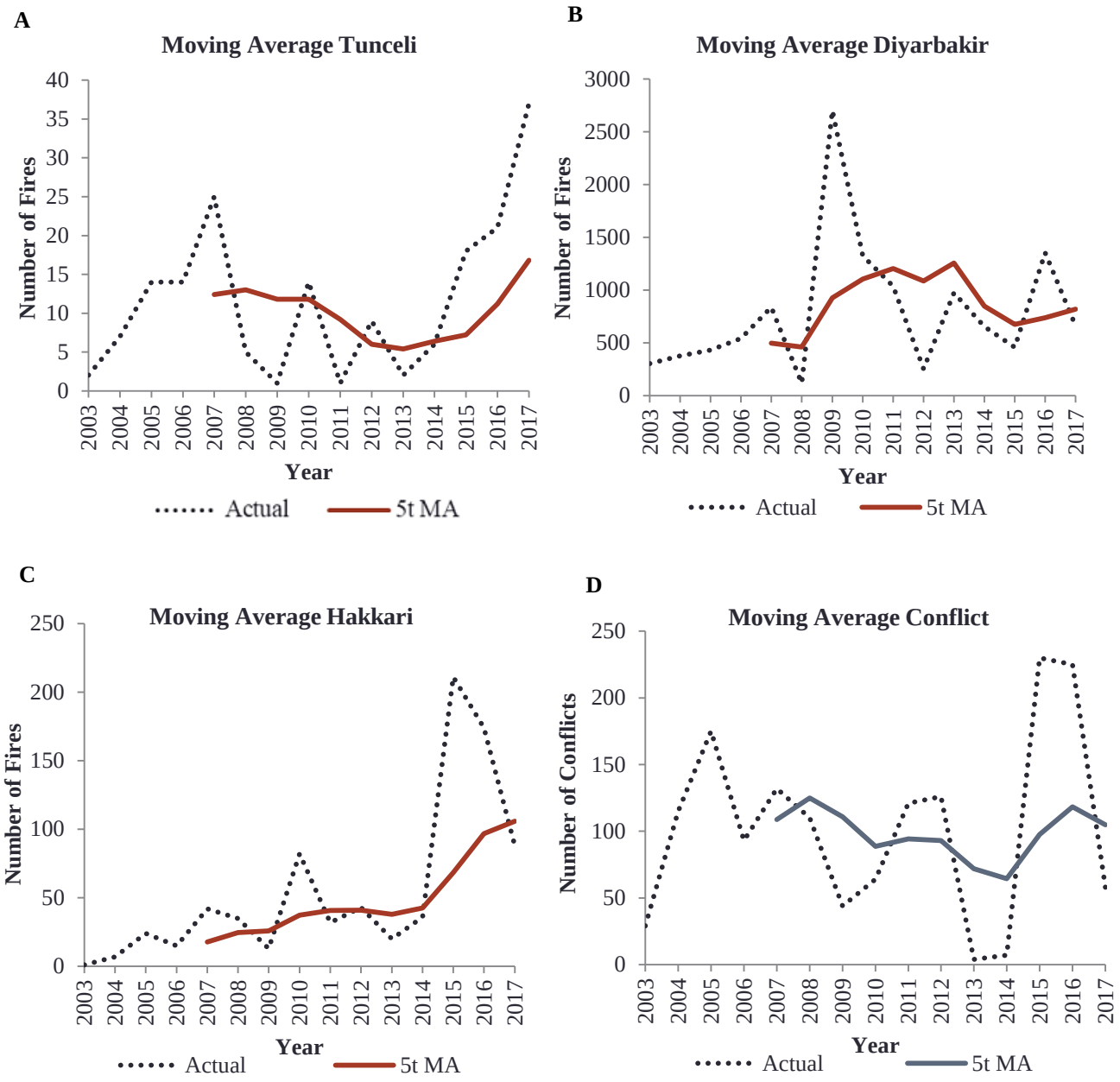

FIGURE 6.2 **A. TUNCELI, B. DIYARBAKIR, C. HAKKARI, D. TURKEY** CHARTS SHOWING THE TRENDS OF NUMBER OF FIRES (A, B, C) AND CONFLICTS (D) FROM 2003 TO 2017. CONFLICT DATA WAS RETRIEVED FROM THE UCDP AND THE FIRE DATA WAS RETRIEVED FROM THE GFED. THE DOTTED LINE, OR ACTUAL, IS THE ORIGINAL TIME SERIES VALUES AND THE SOLID LINE IS THE SMOOTHED 5-TERM MOVING AVERAGE (I.E., 5T MA).

6.3.2 Statistical Analysis and Significance Testing

As described in Section 5.1.1, the Spearman Rank correlation test was used to understand the relationship between the conflict and fire datasets. The results of the test are shown in Table 6.1. The two hypotheses are as follows: H0: there is no statistically significant relationship between the fire and conflict datasets, and H1: there is a statistically significant relationship between the fire and conflict datasets. A p-value ≥ α, rejects H0 and if the p-value < α does not reject H0 (α = 0.05).

For all three areas the null hypothesis is rejected, suggesting that there is a statistically significant relationship between the fire and the conflict datasets. The sign and magnitude of the Spearman's correlation coefficient determine the direction of the relationship. The negative sign of the correlation coefficient for Diyarbakir indicates a statistically significant negative monotonic association and the positive sign for Tunceli and Hakkari indicate a statistically significant positive monotonic association between the fire and conflict data.

Table 6.1 Results from the Spearman rank correlation test between the fire datasets for Tunceli, Diyarbakir, Hakkari, and conflict data for Turkey from 2003 to 2017

	Tunceli	*Diyarbakir*	*Hakkari*
r_s	0.51	-0.13	0.48
p-value	0.05	0.66	0.07
α	0.05	0.05	0.05
Test Result	p ≥ α	p ≥ α	p ≥ α

7. Discussion

Here the results will be discussed referring to the corresponding research question for each part of the research (see Section 1.3.1). In this section the results will be discussed and any relevant additional information will be qualitatively assessed to weave together various elements of the problem and to help address the ongoing narratives.

7.1 Part One Discussion

The change detection technique applied in part three (see Section 5.3) successfully located local fires and characterized severity using high-resolution Sentinel-2 imagery (see Section 6.3). The results found overall, 97% of the total burned area (i.e., 12.05 km^2) from all 13 fires detected, were low to moderately-low burn severity, indicating that all combined effects of the fire had a low environmental impact on the areas (Eidenshink et al. 2007). However, the results are inconclusive because of a lack of validation due to restricted access in the field. In the future,

validation can be carried using high-resolution aerial imagery as reference data in combination with rigorous accuracy assessment methods described in Olofsson (2014).

From the discussion with the locals in the field, the consensus that 'oaks are difficult to burn so the fires have to be purposefully started' is further explored here. In research, it is known that oak-dominated mixed woodlands, as found in Tunceli, are disturbance-tolerant ecosystems and can tolerate low to moderately-low severity fires (Elliott and Vose 2010; Heydari et al. 2016; Harper et al. 2019). In a study by Elliott and Vose (2010) the short-term effects (i.e., one to two years) of prescribed low to moderately-low severity fires on mixed-oak woodlands in mountainous, sub-mesic, environments were observed. The results showed no over-story mortality of trees one to two years after the prescribed burns. In fact, in forest fire management, prescribed low to moderately-low severity fires, which mimic natural disturbance patterns, have been used as a technique to regenerate declining oak populations in the U.S, by removing competitors to aid oak seedling establishment in the understory (Van Lear et al. 2000; Harper et al. 2019). Considering that oak species are generally fire-tolerant, research supports the local's claims that oak trees are 'difficult to burn', although this does not imply anything about the cause of the fires.

Additionally, while the risk for naturally occurring fires should be explored in detail, there are some tools that provide a quick overview of the climate-based wildfire hazard level to help get a better sense of the potential risk. For example, ThinkHazard! (2019) generates location specific reports of general views of the likelihood of hazards in the specified area (http://thinkhazard.org/en/). Using this tool a report generated for Tunceli Province classified the wildfire hazard level as high. This suggests that there is currently a > 50% chance of weather that could support significant wildfires in any given year. Furthermore, the report suggests a likely increase in the frequency of fire weather with the modeled projections of future climate, inclusive of climate change. This high hazard level can partially explain the reason for fires in Tunceli Province. However, no explanation of the cause can be made in certainty without the official establishment of the ignition source during post-burn field assessments.

7.2 Part Two Discussion

VIIRS AF, MODIS AF, and BA all show a large increase in fires after 2015. Incidentally, 2015 is the only observed year where this increase is seen across all three products. VIIRS AF counts increased from an average of 41 counts per year, from 2012 to 2014, to 130 counts per year, from 2015 to 2017. The average MODIS AF counts and BA increased from an average of 5 counts and 1.30 km^2 a year, from 2011 to 2014, to 23 counts and 4.30 km^2 a year from 2015 to 2018.

The increase is consistent with the narratives and also supported by the Joint Research Center (2018) annual technical reports on forest fires. The JRC reported that 2015 was one of the worst fires seasons for all of Turkey in a decade and that 2016 was even worse with a slight improvement in 2017. The report notes that most of the fires in 2016 and 2017 occurred in southeastern Turkey.

Regarding the monthly accounts, the most recent claims of 'strategic burning' in August 2018 (see Section 1.1) can be supported by the 41 fire counts detected by VIIRS and the 5 fire counts detected by MODIS; however, no burned area was detected. In August 2017, 1.50 km^2 of burned area is found, as well as, 111 fires detected by VIIRS, and 5 fires detected by MODIS. These fires are primarily between Kuturderesi, Munzur Valley, and Hozat, which is consistent with the reporting of fires by the Turkish State mentioned in Section 1.1.

Moreover, to understand the validity of the results in context, the accuracy of these products for must be considered. The results of the accuracy assessment for the fire products show high overall accuracies and kappa values (see Section 6.2). The results suggest the data is applicable for applications needing a map accuracy > 90%, which is suitable for this research. However, there are limitations. First, the deficiencies in sample size due to limited availability of fire detections for the MODIS AF and BA products may influence the results and the assessment of multiple years should be considered in future research. Also, only 0.10% of unburned pixels were sampled, which indicates omissions errors may be higher; therefore a preferential sampling strategy to better incorporate errors of omission is desirable.

Furthermore, MODIS BA data suggests that the fires in Tunceli are small, compared with larger fires of over 5 km^2 in other areas of Turkey, distinguished by the Joint Research Center (2018). This has some implications for the reliability of the method used for fire detection. While there is no limit for the size of fire that MODIS can detect, the probability of detection decreases if fires are smaller (Justice et al. 2002). MODIS AF algorithm typically detects active fires that are 50 m^2 to 1000 m^2 in pristine atmospheric conditions (Justice et al. 2002). VIIRS AF product tended to detect more fires than MODIS AF or BA products due to its higher spatial resolution and ability to better detect smaller fires (Schroeder et al. 2014). Still, a large number of both MODIS and VIIRS AF hotspots are detected where MODIS BA is not. This could indicate that the fires are too small to be detected by the MODIS BA algorithm and burned area detection with higher resolution imagery, such as Sentinel-2, is preferable.

However, this study shows that modern techniques in remote sensing are useful for accounting past forest fire occurrences in both time and space. The remote sensing techniques used in this research demonstrated the capabilities for retrospective fire investigation, especially for areas where field work is challenging, and ground data is difficult to obtain.

7.3 PART THREE DISCUSSION

Turkey's conflict data well-represents the political context and conflict dynamics presented in the introduction of the thesis and is suitable for comparison with the fire data. The smoothed fire data exposed the trend of increasing fires detections after the year 2015 for each area of interest. The provinces of Tunceli and Hakkari explicitly show this trend in the data with larger increases in fire accounts relative to the province of Diyarbakir. The trend could be harder to see because Diyarbakir, on average, has many more fires compared to the other provinces. However the reasons for this are unclear. Nonetheless, the general increase in fires after 2015 supports the claims of the locals that the number of fires have increased after the collapse of the peace process in 2015.

The results of the statistical analysis in Section 6.1.2 determined a statistical association or correlation between conflict and fires for all three provinces. This implies that while one variable increases the other variable decreases or increases (i.e., depending on the sign of the Spearman coefficient), perhaps at varying rates (i.e., a nonlinear relationship). The strength and direction of the statistically significant associations are indicated by the correlation coefficients (r_s). Both Tunceli and Hakkari provinces showed moderate positive associations (i.e., r_s = 0.51 and 0.48 respectively) and Diyarbakir Province showed a weak negative association (i.e., r_s = -0.13). Diyarbakir. The negative association for Diyarbakir could be due to an abnormally high number of fires in 2009 (i.e., 2703 fires). Even though Spearman's rank correlation coefficient is less sensitive to outliers than Pearson's correlation coefficients, since the sample size is small the outlier may have enough weight to pull the association in a different direction (Harris 2016). Nonetheless, the association indicates that accounts of fires in these conflict zones and national level conflict dynamics are somehow related. However, to discover more about the nature of the relationship comprehensive data on the causes of the fires is needed.

Furthermore, limitations of the data may influence the results and need to be considered. These limitations include, a lack of validation of the fire data, the small number of years of data available, and the underreporting of conflicts (Sundberg and Melander 2013). First, while a regional validation of the MODIS AF dataset is desirable to ensure that the fires are occurring, more importance is given to understanding general trends of fires and conflicts in this research. Second, the 2003 commission of MODIS Aqua data limits the number of years available. Ideally, at least thirty years of data would be advisable for this type of analysis. Lastly, concerning the conflict data, it is probable that many conflicts are unreported or not found by the UCDP, which may cause an underestimation of conflicts. According to Sundberg and Melander (2013), the UCDP is also limited by strict theoretical definitions of what constitutes a 'conflict event'. UCDP requires organized activities by identifiable actors and does not include armed conflict during semi-organized activities such as riots, protests, or demonstrations. While most

of the conflict data observed in this study are between organized groups such as the PKK and the Turkish State, other conflict events which may influence political tensions are not included. For future research alternatives like the Armed Conflict Location and Event Dataset (ACLED), available for Turkey from 2016, which includes semi-organized conflict, should be considered.

Furthermore, the UCDP geo-referenced conflict data can also be used to find the correlation between the distance of conflict and fire events. Measurements of spatial autocorrelation such as bivariate Moran's I can be used to understand this (Burt et al. 2009). However, in this case, the fires are thought to increase due to heightened political tension and armed conflict at the national-level, and not as a direct repercussion of armed conflict locally. The UCDP does not account for conflict in which the aim is to strategically degrade natural resources and ecosystem services (i.e., animals, trees, water resources…), which would be relevant to this study. Therefore, the data was not used to find the spatial correlation between the conflicts and fires in this study. However, this method could be applied in future research, in areas where fires and conflict are thought to be spatially linked.

8. CONCLUSIONS

The research presents an initial case study demonstrating how modern techniques in remote sensing can be used to contribute quantitative assessments of detailed case studies to better understand impact of conflict on land systems. Furthermore, while the cause of the fires is still unknown, the remote sensing data partially supports the local people's claims that forest fires are occurring in Tunceli Province and have increased after the year 2015.

8.1 FUTURE WORK

A significant challenge in this research is the ability to predict past and present fire occurrences. While a majority of fires in the world are started by humans, natural causes of fires such as lightning or drought as well as societal/anthropogenic predictors must also be taken into consideration. Logistic regression modeling might be useful to understand possible direct and indirect influences or predictors of fire occurrences in conflict areas. Different parameters such as climate, fire risk indexes, or number of media report/tweets can be included (see Figure 8.1).

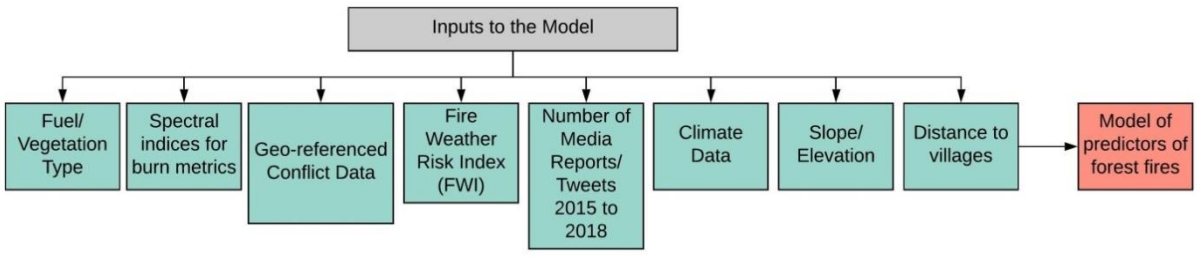

FIGURE 8.1 POTENTIAL INPUTS FOR THE LOGISTIC REGRESSION MODEL PROPOSED TO PREDICT FOREST FIRE OCCURRENCE IN THE AREA(S) OF INTEREST DISCUSSED FOR FUTURE WORK

9. REFERENCES

350 Ankara. 2018. Bir yerden değil, pek çok yerden #DersimYanıyor. Oradaki kurdun, kuşun ağacın, canı yok mu? *Twitter*.

Achard, F., and M. C. Hansen. 2017. *Global Forest Monitoring from Earth Observation*. 1st ed. Boca Raton, FL, USA: CRC Press, Inc.

Adger, W. N., J. M. Pulhin, J. Barnett, G. D. Dabelko, G. K. Hovelsrud, M. Levy, U. O. Spring, and C. H. Vogel. 2014. Human Security. In *Climate Change 2014: Impacts, Adaptation, and Vulnerability. Part A: Global and Sectoral Aspects. Contribution of Working Group II to the Fifth Assessment Report of the Intergovernmental Panel on Climate Change*, 755–791.

Amnesty International. 1994. *Turkey A policy of Denial*. Vol. 985.

Balta, E. 2005. The Ceasefire This Time. *Middle East Research and Information Project*.

Baran, M., M. Yldrm, and A. Ylmaz. 2011. Evaluation of ecological design strategies in traditional houses in Diyarbakir, Turkey. *Journal of Cleaner Production* 19: 609–619. doi:10.1016/j.jclepro.2010.11.001.

Baumann, M., and T. Kuemmerle. 2016. The Impacts of Warfare and Armed Conflict on Land Systems. *Journal of Land Use Science*. Taylor & Francis: 1–17. doi:10.1080/1747423X.2016.1241317.

Burt, J., G. Barber, and D. Rigby. 2009. *Elementary Statistics for Geographers*. Third. New York, New York, USA: The Guilford Press.

Camilla, S., A. Rustad, J. Ketil, W. Larsen, and N. Petter. 2008. Foliage and fighting : Forest resources and the onset , duration , and location of civil war. *Political Geography* 27. Elsevier: 761–782. doi:10.1016/j.polgeo.2008.09.004.

Central Intelligence Agency. 2019. Turkey. *The World Factbook*.

Chuvieco, E. 2009. *Earth Observation of Wildland Fires*. Edited by Emilio Chuvieco. Vol. 91. Berlin, Heidelberg: Springer.

Chuvieco, E., J. Lizundia-Loiola, M. Lucrecia Pettinari, R. Ramo, M. Padilla, K. Tansey, F. Mouillot, P. Laurent, et al. 2018. Generation and analysis of a new global burned area product based on MODIS 250 m reflectance bands and thermal anomalies. *Earth System Science Data* 10: 2015–2031. doi:10.5194/essd-10-2015-2018.

climate-data.org. 2019. Climate Data for Cities Worldwide. *climate-data.org*.

Congalton, R. G., and K. Green. 2009. *Assessing the Accuracy of Remotely Sensed Data*. Second. Boca Raton, FL, USA: CRC Press, Inc.

Copernicus Research and User Support. 2017. Burned Area Mapping with Sentinel-2 using SNAP. ESA.

Crisis Group. 2019. Turkey's PKK Conflict: A Visual Explainer. *International Crisis Group*.

Dahlman, C. 2008. The Political Geography of Kurdistan. *Eurasian Geography and Economics* 43: 271–299. doi:10.2747/1538-7216.43.4.271.

Defourny, P. 2017. *Land Cover CCI Product User Guide Version 2.0*.

Eidenshink, J., B. Schwind, K. Brewer, Z. Zhu, B. Quayle, S. Howard, and S. Falls. 2007. A Project For Monitoring Trends in Burn Severity. *Ecology* 3: 3–21.

Ekurd Daily. 2011. Kurdish PKK leader: We will not withdraw our autonomy demand. *Ekurd Daily News*.

Elliott, K. J., and J. M. Vose. 2010. Short-term effects of prescribed fire on mixed oak forests in the southern Appalachians: vegetation response. *The Journal of the Torrey Botanical Society* 137: 49–66. doi:10.3159/09-ra-014.1.

Eroglu, V., and I. Üzmez. 2015. *Türkıye Orman Varlığı 2015*.
European Space Agency. 2015. *Sentinel-2 User Handbook*.
Fisher, R. A. 1934. *Statistical Methods for Research Workers*. 5th ed. Edinburgh: Oliver and Boyd.
Fornacca, D., G. Ren, and W. Xiao. 2017. Performance of Three MODIS fire products (MCD45A1, MCD64A1, MCD14ML), and ESA Fire_CCI in a mountainous area of Northwest Yunnan, China, characterized by frequent small fires. *Remote Sensing* 9: 1–21. doi:10.3390/rs9111131.
George, D., and M. Mallery. 2010. *SPSS for Windows Step by Step: A Simple Guide and Reference, 17.0 update*. 17.0. Boston: Pearson.
Giglio, L., J. Descloitres, C. O. Justice, and Y. J. Kaufman. 2003. An enhanced contextual fire detection algorithm for MODIS. *Remote Sensing of Environment* 87: 273–282. doi:10.1016/S0034-4257(03)00184-6.
Giglio, L., W. Schroeder, and C. O. Justice. 2016. The collection 6 MODIS active fire detection algorithm and fire products. *Remote Sensing of Environment* 178. British Geological Survey, NERC: 31–41. doi:10.1016/j.rse.2016.02.054.
Giglio, L., L. Boschetti, D. Roy, A. A. Hoffman, and M. Humber. 2018a. Collection 6 MODIS Burned Area product User Guide. *Nasa*: 1–26. doi:10.1016/j.jhsb.2003.12.010.
Giglio, L., L. Boschetti, D. P. Roy, M. L. Humber, and C. O. Justice. 2018b. The Collection 6 MODIS burned area mapping algorithm and product. *Remote Sensing of Environment* 217. Elsevier: 72–85. doi:10.1016/j.rse.2018.08.005.
Hanson, T. 2018. Biodiversity conservation and armed conflict : a warfare ecology perspective 1429: 50–65. doi:10.1111/nyas.13689.
Harper, J. M., R. B. Standiford, and J. W. LeBlanc. 2019. The Role of Fire in California's Oak Woodlands -. *Oak Woodland Management - University of California*.
Harris, R. 2016. *Quantitative Geography: The Basics*. Edited by Robert Rojek. Thousand Oaks: SAGE Publications Inc.
HDP. 2015. *Observations and Technical Review Report on Forest Fire*.
Heydari, M., M. Faramarzi, and D. Pothier. 2016. Post-fire recovery of herbaceous species composition and diversity, and soil quality indicators one year after wildfire in a semi-arid oak woodland. *Ecological Engineering* 94. Elsevier B.V.: 688–697. doi:10.1016/j.ecoleng.2016.05.032.
International Crisis Group. 2012. *Turkey: The PKK and a Kurdish Settlement*.
Joint Research Center. 2018. *Forest Fires in Europe , Middle East and North Africa 2017*. 2017th ed. Ispra: European Commission. doi:10.2788/99870.
Jongerden, J. 2010. Village Evacuation and Reconstruction in Kurdistan (1993-2002). *Études rurales*: 77–100.
Jongerden, J., H. De Vos, and J. Van Etten. 2007. Forest Burning as Counterinsurgency in Turkish-Kurdistan: An analysis from space. *International Journal of Kurdish Studies* 21: 1–15.
Justice, C. O., L. Giglio, S. Korontzi, J. Owens, J. T. Morisette, D. Roy, J. Descloitres, S. Alleaume, et al. 2002. The MODIS fire products. *Remote Sensing of Environment* 83. Elsevier: 244–262. doi:10.1016/S0034-4257(02)00076-7.
Key, C. H., and N. C. Benson. 2006. Landscape Assessment: Ground measure of severity, the Composite Burn Index; and Remote sensing of severity, the Normalized Burn Ratio. *Other Government Series* RMRS-GTR-1.

Köse, T. 2017. Rise and fall of the AK party's kurdish peace initiatives. *Insight Turkey* 19: 139–165. doi:10.25253/99.2017192.08.

Landis, J. R., and G. G. Koch. 1977. The Measurement of Observer Agreement for Categorical Data Data for Categorical of Observer Agreement The Measurement. *Biometrics* 33: 159–174.

Van Lear, D. H., P. H. Brose, and P. D. Keyser. 2000. Using Prescribed Fire to Regenerate Oaks. In *Workshop on Fire, People, and the Central Hardwoods Landscape*, 97–102.

Lillesand, T. M., and R. W. Kiefer. 1994. *Remote sensing and image interpretation.* 3. ed. Wiley & Sons.

Machlis, G. E., and T. Hanson. 2008. Warfare Ecology 58: 729–736.

McFeeters, S. K. 1996. The use of the Normalized Difference Water Index (NDWI) in the delineation of open water features. *International Journal of Remote Sensing* 17: 1425–1432. doi:10.1080/01431169608948714.

Melorose, J., R. Perroy, and S. Careas. 2015. *Earth Observation ofWildland Fires in Mediterranean Ecosystems*. *Statewide Agricultural Land Use Baseline 2015*. Vol. 1. doi:10.1017/CBO9781107415324.004.

National Parks Of Turkey. 2019. Munzur Valley National Park. *National Parks*. http://www.nationalparksofturkey.org/munzur-valley-national-park-en. Accessed May 10.

Nurcan Baysal. 2018. Kurdish geography is burning and Turkish environmentalists stand watching. *Ahval*.

Olofsson, P., G. M. Foody, M. Herold, S. V. Stehman, C. E. Woodcock, and M. A. Wulder. 2014. Good practices for estimating area and assessing accuracy of land change. *Remote Sensing of Environment* 148. Elsevier Inc.: 42–57. doi:10.1016/j.rse.2014.02.015.

Pallant, J. 2005. *SPSS Survival Manual: A step by step guide to data analysis using SPSS*. 2nd ed. Crows Nest NSW: Allen & Unwin.

Parks, S. A., G. K. Dillon, and C. Miller. 2014. A new metric for quantifying burn severity: The relativized burn ratio. *Remote Sensing* 6: 1827–1844. doi:10.3390/rs6031827.

Quayle, B., C. Albury, and J. Lecker. 2010. *Imagery support*.

Regional IM Working Group - Europe. 2019. Turkey - Administrative Boundaries (Levels 0, 1, 2). *Humanitarian Data Exchange*.

Roteta, E., A. Bastarrika, M. Padilla, T. Storm, and E. Chuvieco. 2019. Development of a Sentinel-2 burned area algorithm: Generation of a small fire database for sub-Saharan Africa. *Remote Sensing of Environment* 222. Elsevier: 1–17. doi:10.1016/j.rse.2018.12.011.

San-Miguel-Ayanz, J., N. Ravail, V. Kelha, and A. Ollero. 2005. Active fire detection for fire emergency management: Potential and limitations for the operational use of remote sensing. *Natural Hazards* 35: 361–376. doi:10.1007/s11069-004-1797-2.

Schroeder, W., and L. Giglio. 2016. Visible Infrared Imaging Radiometer Suite (VIIRS) 750 m Active Fire Detection and Characterization Algorithm Theoretical Basis Document: 0–21.

Schroeder, W., P. Oliva, L. Giglio, and I. A. Csiszar. 2014. Remote Sensing of Environment The New VIIRS 375 m active fi re detection data product : Algorithm description and initial assessment. *Remote Sensing of Environment* 143. Elsevier Inc.: 85–96. doi:10.1016/j.rse.2013.12.008.

Shapiro, S. S., and M. B. Wilk. 1965. An Analysis of Variance Test for Normality (Complete Samples). *Biometrika* 52: 591–611.

SNK. 1994. *Forced Evacuations and Destruction of Villages in Dersim (Tunceli), and Western Bingöl , Turkish Kurdistan*. Amsterdam.

Spearman, C. 1904. The Proof and Measurement of Association between Two Things: The American Journal of Psychology. *The American journal of psychology* 15: 72–101. doi:10.1037/h0065390.

Stockholm Center for Freedom. 2018. Turkish military allegedly set forest fires around Tunceli province. *News*.

Sundberg, R., and E. Melander. 2013. Introducing the UCDP Georeferenced Event Dataset. *Journal of Peace Research* 50: 523–532. doi:10.1177/0022343313484347.

T.C. Hakkari Governorship. 2019. Geographical Structure. http://www.hakkari.gov.tr/tarihce-ve-cografi-yapi. Accessed March 28.

TC Tunceli Governorship. 2017. Press Release 11.08.2017. *Press Release*.

TC Tunceli Governorship. 2019. TC Tunceli Governorship.

Tekinoğlu, D. 2017. *Bindokuzyüzdoksandört*. Turkey: TIHV Insan Haklari Belgesel Film Günleri.

teyit. 2018. Fotoğrafın, Ağustos 2018'de Tunceli'de çıkan yangın sırasında çekildiği iddiası doğru değil. Fotoğraf, 2015 yılında Tunceli, Mardin ve Şırnak'ta çıkan yangınlar sırasında çekilmiş. 2017'de #DersimYanıyor etiketiyle internette yayılan 6 yanlış görüntü: htt. *Twitter*.

The Kurdish Project. 2019. Diyarbakir. https://thekurdishproject.org/kurdistan-map/turkish-kurdistan/diyarbakir/. Accessed May 10.

ThinkHazard! 2019. *Tunceli, Turkey - ThinkHazard!*

Tunceli Governor. 2018. Press Briefing. *News from the Governor*.

Turkish Statistical Institute. 2018. Statistical Indicators.

UNESCO World Heritage Centre. 2015. Diyarbakır Fortress and Hevsel Gardens Cultural Landscape. *World Heritage List*.

USDI National Park Service. 2003. Fire Monitoring Handbook. *Fire Monitoring Handbook*: 274.

USGS. 2004. *Nps-usgs national burn severity mapping project working group*. Sioux Falls.

USGS. 2019. What is remote sensing and what is it used for? https://www.usgs.gov/faqs/what-remote-sensing-and-what-it-used?qt-news_science_products=7#qt-news_science_products. Accessed January 20.

Wooster, M. J., G. Roberts, A. M. S. Smith, J. Johnston, P. Freeborn, S. Amici, and A. T. Hudak. 2013. *Thermal Infrared Remote Sensing*. Vol. 17. doi:10.1007/978-94-007-6639-6.

World Wildlife Fund. 2019a. Ecoregions.

World Wildlife Fund. 2019b. Turkey Ecoregions.

Yalanlari, G. 2017. #DersimYanıyor diye paylaşılan fotoğraf asılsızdır. Görsel 2003 yılında yurtdışında yaşanan bir orman yangınına ait. https://www.b.dk/verden/skovbrande-i-californien-de-vaerste-nogensinde …. *Twitter*.

10. SUPPLEMENTARY DATA

APPENDIX A

TABLE 1A. PRIMARY WAVELENGTHS USED IN FIRE DETECTION FOR EACH PRODUCT

MODIS BA Algorithm				
Channel	**Type**	**Central Wavelength**	**Resolution**	**Purpose**
1	Red	0.65	250	Threshold to override cloud commission error in the MOD09 internal cloud mask
5	SWIR	1.24	500	For burn sensitive vegetation index
7	SWIR	2.13	500	For burn sensitive vegetation index
MODIS AF Algorithm				
Channel	**Type**	**Central Wavelength**	**Resolution**	**Purpose**
1	Red	0.65	250	Sunglint and coastal false alarm rejection; cloud masking
2	NIR	0.86	250	Bright surface, sun glint, and coastal false alarm rejection; cloud masking
7	SWIR	2.1	500	Sunglint and coastal false alarm rejection
21	MWIR	4	1000	High-range channel for active fire detection
22	MWIR	4	1000	Low-range channel for active fire detection
31	Thermal	11	1000	Active fire detection, cloud masking
32	Thermal	12	1000	Cloud masking
VIIRS AF Algorithm				
Channel	**Type**	**Central Wavelength**	**Resolution**	**Purpose**
I1	Red	0.64	375	Cloud and water classification
I2	NIR	0.86	375	Cloud and water classification
I3	SWIR	1.61	375	Water classification
I4	MWIR	3.75	375	Fire detection
M13	MWIR	4	750	FRP retrieval, fire detection over water and across the South Atlantic magnetic anomaly region
I5	Thermal	11.45	375	Fire detection and cloud classification
Sentinel Burn Severity Mapping				
Channel	**Type**	**Central Wavelength**	**Resolution**	**Purpose**
B3	Green	0.56	10	Water and cloud mask
B8	NIR	0.83	10	For burn sensitive vegetation index; water and cloud mask
B12	SWIR	2.2	20	For burn sensitive vegetation index

TABLE 2A. DETAILS OF SATELLITE SOURCES OF LAND COVER DATA

Land Cover Database	Reference Period	Spatial Coverage and Resolution	Satellite Data Source
ESA CCI Global Annual Land Cover Maps	2014 - 2015	Global/300m	• Baseline 10-year global LC map • PROBA-V global surface reflectance composites at 1 km for years 2014 and 2015 for up-dating baseline • PROBA-V time series at 300 m for 2014 and 2015 to delineate the identified changes in the LC map spatial resolution

TABLE 3A. BURN SEVERITY TOTALS FOR FIRES DETECTED FROM 2016 TO 2018

ID	Year	Location(s)	Burn Date	Pre-Burn Image	Post-Burn Image	BA Total (km^2)	BA Low (km^2)	BA Moderate-Low (km^2)	BA Moderate-High (km^2)	BA High (km^2)
1	2015	Hozat District, Noydasi Village	24/07/15	-	-	-	-	-	-	-
2	2015	Kocakoc Village, Ambar Village	05/08/15	-	-	-	-	-	-	-
3	2015	Nazimiye District, Bezik Forests	23/08/15	-	-	-	-	-	-	-
4	2015	Inonu Neighborhood, Pah hamlet	23/08/15	-	-	-	-	-	-	-
F5	2016	Ovacik District, Sultan Baba Mountain	10/08/16	08/01/16	08/11/16	1.79	0.90	0.69	0.20	0.0002
F6	2016	Nazimiye District, Dereova Village, Dokuz Kaya Village	28/08/16	21/08/16	31/08/16	0.97	0.83	0.14	0.01	0.00
F7	2017	Kutuderesi, Gokcek Village	09/08/17 - 12/08/17	08/06/17	26/08/17	0.86	0.79	0.07	0.01	0.00
F8	2017	Ovacik District, Ahponos Valley	09/08/17 - 12/08/17	08/06/17	26/08/17	0.09	0.05	0.04	0.00	0.00
F9/F10	2017	Geyiksuyu/Sin Village area	09/08/17 - 12/08/17	08/06/17	26/08/17	4.78	3.58	1.09	0.11	0.0004
F11	2017	Hozat District, Alibogazi	09/08/17 - 12/08/17	08/06/17	26/08/17	0.20	0.18	0.01	0.00	0.00
F12	2018	Pertek District, Cataksu Village	27/07/18	17/07/18	08/01/18	0.06	0.06	0.00	0.00	0.00
F13	2018	Hozat District, Alibogazi	15/08/18	08/01/18	26/08/18	3.28	2.94	0.32	0.03	0.0010
					Total	12.05	9.33	2.35	0.37	0.0016

TABLE 4A. SUMMARIZED/ DIGITIZED FIELD OBSERVATION NOTES FOR NINE FIELD LOCATIONS IN TUNCELI PROVINCE APRIL 2019

Fire	F1P1	F1P2	F1P2.2	F1P3	F1P4	F1P5	F2P1	F2P2	F3P1
Date of visit	20/04/19	20/04/19	20/04/19	20/04/19	20/04/19	20/04/19	21/04/19	21/04/19	22/04/19
Year (local claim)	2018	2018	2018	2018	2018	2017	2016	2017	2018
Duration (local claim)	1 week	7 to 10 days	7 to 10 days	unknown	unknown	few days	unknown	unknown	unknown
Extinction	on its own	on its own	on its own	unknown	unknown	locals	unknown	locals	unknown
Coordinates	39.17116, 39.4573	39.16008, 39.43898	39.1513291, 39.4148583	39.15668, 39.37617	39.20769, 39.23066	39.33978, 39.21973	39.10477, 39.62533	39.18954, 39.67664	39.10755, 39.41011
Area Approximation	500 to 800 m^2	500 m^2	200 to 400 m^2	500,000 ha	500 m^2 ?	> 500 m^2	> 500 m^2	> 500 m^2	> 500 m^2
Cause (local claim)	police	unknown	unknown	unknown	unknown	military operations, helicopter bombs	unknown	small bomb used by military	unknown
Terrain	foot of mountain	slope of mountain	slope, foot of mountain, valley, flat areas	mountainous	high mountainous	mountainous	hillslope	mountainous	mountainous
Road	Tunceli Hozat Yolu	Tunceli Hozat Yolu	Tunceli Hozat Yolu	Tunceli Hozat Yolu	Ovacik Hozat Yolu	Ovacik Hozat Yolu	Karakoc Yolu	unnamed road off Erzincan Tunceli Yolu	n/a
Nearest Village	Halvori (Krarsilar)	Halvori (Krarsilar)	Sinmera, Geyiksuyu Mecra, Pinarlar	Geyiksuyu	Yuceldi	Ovacik	Pax area, Sinon koyu	Kutu Deresi Kpr	Cilga?
Landcover Type	oak dominated forest/ shrubland	forest or shrubland	shrubland	oak dominated shrubland	mix of birch and oak	n/a	oak dominated shrubland	forested?	n/a

TABLE 5A. VIIRS AF INTERNAL QUALITY ASSESSMENT

VIIRS AF			
	Confidence Levels	**Fire Counts**	***%***
Low (l)	Daytime fire pixels associated with areas of sun glint and lower relative temperature anomaly (<15K) in I4	99	14.31
Nominal (n)	Free of sunglint during the day and marked by strong (>15k) temperature anomaly in either day or nighttime data.	549	79.34
High (h)	Fire pixels associated with day or nighttime saturated pixels	44	6.36
Total		692	100

TABLE 6A. MODIS AF INTERNAL QUALITY ASSESSMENT

MODIS AF	
Day/Night	
Day	93
Night	25
Satellite	
Aqua	59
Terra	59
Confidence	
Mean	61.67
Median	63
Mode	62
Standard Deviation	18.5
Range	100
Minimum	0
Maximum	100
Count	118

FIGURE 1A. UN LCCS LEGEND

Value	Label	Color
0	No Data	
10	Cropland, rainfed	
11	Herbaceous cover	
12	Tree or shrub cover	
20	Cropland, irrigated or post-flooding	
30	Mosaic cropland (>50%) / natural vegetation (tree, shrub, herbaceous cover) (<50%)	
40	Mosaic natural vegetation (tree, shrub, herbaceous cover) (>50%) / cropland (<50%)	
50	Tree cover, broadleaved, evergreen, closed to open (>15%)	
60	Tree cover, broadleaved, deciduous, closed to open (>15%)	
61	Tree cover, broadleaved, deciduous, closed (>40%)	
62	Tree cover, broadleaved, deciduous, open (15-40%)	
70	Tree cover, needleleaved, evergreen, closed to open (>15%)	
71	Tree cover, needleleaved, evergreen, closed (>40%)	
72	Tree cover, needleleaved, evergreen, open (15-40%)	
80	Tree cover, needleleaved, deciduous, closed to open (>15%)	
81	Tree cover, needleleaved, deciduous, closed (>40%)	
82	Tree cover, needleleaved, deciduous, open (15-40%)	
90	Tree cover, mixed leaf type (broadleaved and needleleaved)	
100	Mosaic tree and shrub (>50%) / herbaceous cover (<50%)	
110	Mosaic herbaceous cover (>50%) / tree and shrub (<50%)	
120	Shrubland	
121	Evergreen shrubland	
122	Deciduous shrubland	
130	Grassland	
140	Lichens and mosses	
150	Sparse vegetation (tree, shrub, herbaceous cover) (<15%)	
152	Sparse shrub (<15%)	
153	Sparse herbaceous cover (<15%)	
160	Tree cover, flooded, fresh or brakish water	
170	Tree cover, flooded, saline water	
180	Shrub or herbaceous cover, flooded, fresh/saline/brakish water	
190	Urban areas	
200	Bare areas	
201	Consolidated bare areas	
202	Unconsolidated bare areas	
210	Water bodies	
220	Permanent snow and ice	

TABLE 7A: MODIS BA YEARLY AND MONTHLY TOTALS FOR TUNCELI PROVINCE FROM 2010 TO 2018 (EXTENDED DRY SEASON)

Year	May km^2	June km^2	July km^2	August km^2	September km^2	October km^2	Yearly Total
2010	0.00	0.00	0.00	0.00	0.00	0.00	0.00
2011	0.00	0.64	1.29	0.00	0.00	0.64	2.58
2012	0.00	0.00	0.21	0.00	0.00	0.00	0.21
2013	0.00	0.86	0.43	0.00	0.21	0.86	2.36
2014	0.00	0.00	0.00	0.00	0.00	0.00	0.00
2015	0.43	0.21	0.64	0.21	0.64	0.00	2.15
2016	0.00	0.00	1.07	1.29	3.22	0.00	5.58
2017	0.00	0.00	0.00	1.50	2.79	0.21	4.51
2018	0.00	1.07	0.00	0.00	2.79	1.50	5.37
Monthly Totals	0.43	2.79	3.65	3.01	9.66	3.22	22.75

TABLE 8A. MODIS AF YEARLY AND MONTHLY TOTALS FOR TUNCELI PROVINCE FROM 2010 TO 2018 (EXTENDED DRY SEASON)

MODIS AF

Year	Count	Year	May	June	July	August	September	October
2010	7	**2010**	0	0	0	7	0	0
2011	5	**2011**	0	0	0	3	0	2
2012	8	**2012**	0	0	0	3	4	1
2013	2	**2013**	0	0	1	0	1	0
2014	5	**2014**	0	0	0	2	3	0
2015	14	**2015**	0	0	5	1	8	0
2016	13	**2016**	0	0	1	10	2	0
2017	38	**2017**	0	0	0	17	19	2
2018	26	**2018**	0	0	2	5	19	0
Total	106	**Total**	0	0	9	38	56	3

TABLE 9A. VIIRS ACTIVE FIRE DATA YEARLY AND MONTHLY TOTALS FOR TUNCELI PROVINCE FROM 2012 TO 2018 (EXTENDED DRY SEASON)

VIIRS AF

Year	Count	Year	May	June	July	August	September	October
2012	64	**2012**	0	1	2	19	35	7
2013	33	**2013**	1	0	2	5	19	6
2014	26	**2014**	2	1	4	11	7	1
2015	87	**2015**	0	0	33	17	36	1
2016	71	**2016**	0	0	16	31	9	15
2017	233	**2017**	0	0	2	111	108	12
2018	178	**2018**	0	0	14	41	123	0
Total	692	Total	3	2	73	235	337	42

TABLE 10A. AREA BURNED (KM^2) PER VEGETATION CLASS FOR EACH YEARLY EXTENDED DRY SEASON. LAND COVER CLASSES EXTRACTED FROM THE 2015 ESA-CCI-LC BASED ON THE UN-LCCS

Land Cover Classes	2018	2017	2016	2015	2014	2013	2012	2011	2010	Class Total
Mosaic natural vegetation (tree, shrub, herbaceous) > 50%	0.86	2.15	0.43	0.00	0.00	0.00	0.21	0.00	0.00	3.65
Mosaic tree and shrub > 50%	0.00	0.43	0.86	0.00	0.00	0.21	0.00	0.00	0.00	1.50
Grassland	0.64	0.21	1.07	1.07	0.00	0.64	0.00	0.86	0.00	4.50
Sparse Vegetation (tree, shrub, herb) < 15%	0.64	0.00	0.00	0.21	0.00	0.21	0.00	0.00	0.00	1.07

TABLE 11A. 16 KURTOSIS AND SKEWNESS VALUES OF THE FIRE AND CONFLICT DATASETS (2003 TO 2017) FOR EACH AREA OF INTEREST (TUNCELI, DIYARBAKIR, HAKKARI, TURKEY)

Datasets 2003 to 2017	Tunceli AF	Diyarbakir AF	Hakkari AF	Turkey Conflict
Kurtosis	0	5	2	2
Skewness	1	2	2	2

TABLE 12A. RESULTS FROM SHAPIRO-WILK TEST FOR NORMALITY FOR TUNCELI, DIYARBAKIR, HAKKARI, AND TURKEY FIRE AND CONFLICT DATASETS (2003 TO 2018)

Shapiro-Wilk Test for Normality Results				
	Tunceli	**Diyarbakir**	**Hakkari**	**Turkey**
	Fire	**Fire**	**Fire**	**Conflict**
SS	1103.73	2055104.00	29421.60	69694.40
b	31.81	1380.09	155.67	256.58
W	0.92	0.93	0.82	0.94
p-value	0.01	0.24	0.01	0.44
alpha	0.05	0.05	0.05	0.05

SS	the sum of squares of deviations of the data points from their sample mean
b	the summed difference of smallest and largest ranked values multiplied by a coefficient
W	b^2/SS
p-value	statistical probability
alpha	level of significance

FIGURE 2A. SCATTER PLOT OF FIRE AND CONFLICT DATASETS FOR EACH AREA OF INTEREST (I.E. TUNCELI, DIYARBAKIR, HAKKARI, TURKEY) FOR YEARS 2003 TO 2018 (SEE SECTION 5.1)

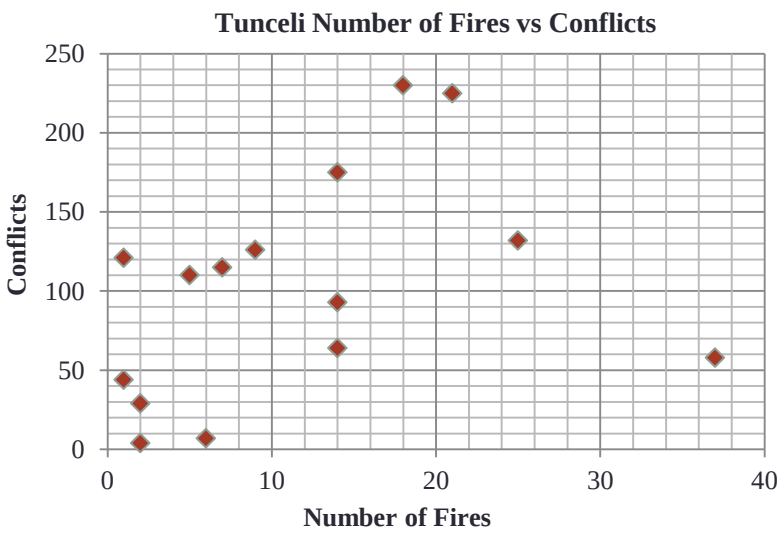

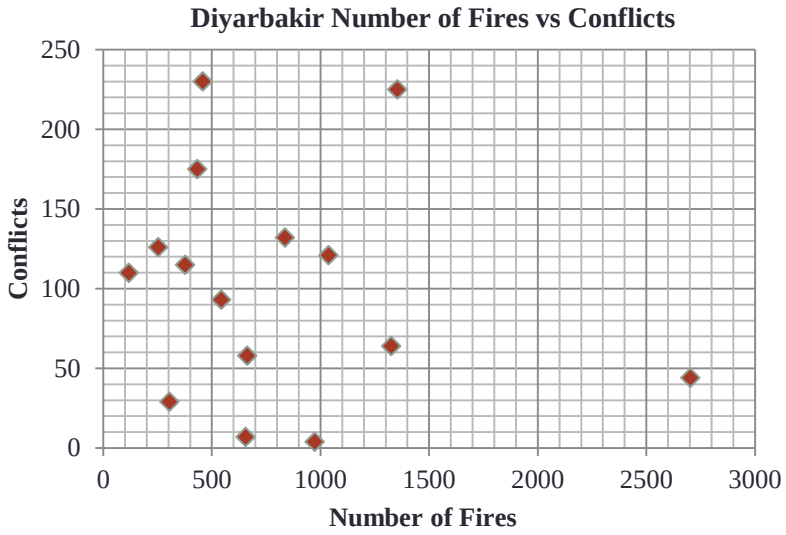

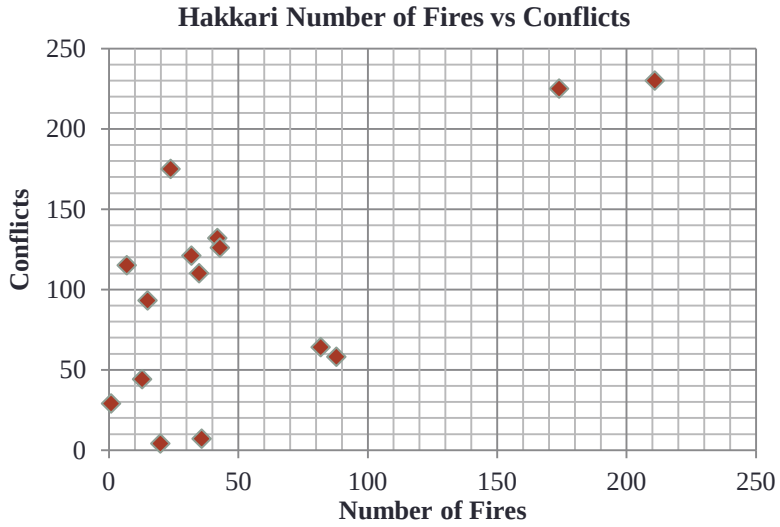

APPENDIX B

FIRE PROJECT FIELD OBSERVATIONS:
RECONNAISSANCE MONITORING
Date and Time:
Monitor's Name:
Recent\Current Weather (Rain? Cloud?):
Route:
Nearest Village:

Name/Number/ Map Coordinates	Name: Number: Coordinates:
Location/ Size/ Field Coordinates *Approximate size?*	
Size of Area Assessed?	
Terrain *Mountainous, valley, plateau, flat?*	
Aspect *North, East, West, South facing?*	Multiple? Yes / No North / East / West / South
Slope *Steep, moderate, mild?*	Steep / Moderate / Mild

LandCover Type *Forest or woodland? Brush or shrubland? Grassland?*	
Wildlife Habitat? *Animals, burrows found?*	
Nearby Water Resources? *Lakes, streams, rivers?*	
Evidence of a fire? *Yes or no?*	Yes / No
Fire Cause Known? *Ignition? origin of fire?*	
Duration Known? *How long did the fire last?*	
Fire extinction? *How was the fire put out?*	
Fuels and Vegetation Description *Describe the fuels array, composition, and dominant vegetation of the burn area. If possible, determine primary fuel models: fuel models #1–13 (Anderson 1982)*	

Vegetation Stress or Scorch Marks? *Yes or no? Average char height? Surface, understory, overstory?*	Yes / No Surface / Understory / Overstory Char Height:
Vegetation Frequency? *Frequency is a measure of the abundance and distribution of a species. Not easily visualized.*	Most Frequent: Frequent: Less Frequent:
Vegetation Density? *Density is the number of individuals per unit area. Density is independent of cover, the proportion of area covered by vegetation.*	Density of All Vegetation: High / Medium / Sparse Patches: Yes / No Grouped Species:
Vegetation Cover? *One of the most commonly used types of cover is canopy cover, which is expressed as a percentage of the total area measured, and defined as the vertical projection of vegetation onto the ground surface, when viewed from above*	Canopy Cover: Full / Moderate / Less Understory Cover: Full / Moderate / Less Surface Cover: Full / Moderate / Less
Litter Depth? *Measure with ruler*	

Top Soil Characteristics?	Color: Texture: Fine / Medium / Course Mineral or Organic
Live Vegetation Damage? *Shrubs, trees, herbaceous? Relative number alive. Crown and pole damages. % scorched? Young or old?*	Type(s): % Damaged: Other:
Dead Vegetation Damage? *Shrubs, trees, herbaceous? Relative number dead. Crown and pole damages*	Type(s): % Dead: Other:
Regrowth? *Seedling present or new vegetation found?*	Yes / No Type(s): Age Approximation:
Other Objects Burned?	
Claims of locals?	
Photographs? *A coded photograph identification 'card' should be prepared.*	

Raise the camera to a height of 4 ft. On a hillside, angle the camera with the slope. Align the camera horizontally for the recommended photos. Take an additional vertical shot, if that better characterizes the plot. Do not include sky.	

Table 3. Recommended Standard variables for monitoring (level 3 & 4) grassland, brush, and forest plots.

Plot Type	Variables
Grassland	• Percent cover by species • Relative cover by species • Number of non-native species • Number of native species • Burn severity
Brush or Shrubland	All grassland variables, plus • Shrub density by species • Shrub age by species
Forest or Woodland	All grassland and brush variables, plus • Tree density by species • Tree diameter by species • Fuel load by size class • Total fuel load • Duff depth • Litter depth • Average scorch height • Percent of crown scorched

Other Notes:

Reference:

Fire Monitoring Handbook: National Park Service U.S. Department of the Interior

USDI National Park Service. 2003. Fire Moni-Park Service to document basic information, to detect toring Handbook. Boise (ID): Fire Manage-trends, and to ensure that each park meets its fire and ment Program Center, National Interagency resource management objectives. From identified Fire Center. 274p.

Department of Physical Geography and Ecosystem Science, Lund University

Lund University GEM thesis series are master theses written by students of the international master program on Geo-information Science and Earth Observation for Environmental Modelling and Management (GEM). The program is a cooperation of EU universities in Iceland, the Netherlands, Poland, Sweden and UK, as well a partner university in Australia. In this series only master thesis are included of students that performed their project at Lund University. Other theses of this program are available from the ITC, the Netherlands (www.gem-msc.org or www.itc.nl).

The student thesis reports are available at the Geo-Library, Department of Physical Geography and Ecosystem Science, University of Lund, Sölvegatan 12, S-223 62 Lund, Sweden. Report series started 2013. The complete list and electronic versions are also electronic available at the LUP student papers (https://lup.lub.lu.se/student-papers/search/) and through the Geo-library (www.geobib.lu.se).

1 Soheila Youneszadeh Jalili (2013) The effect of land use on land surface temperature in the Netherlands

2 Oskar Löfgren (2013) Using Worldview-2 satellite imagery to detect indicators of high species diversity in grasslands

3 Yang Zhou (2013) Inter-annual memory effects between Soil Moisture and NDVI in the Sahel

4 Efren Lopez Blanco (2014) Assessing the potential of embedding vegetation dynamics into a fire behaviour model: LPJ-GUESS-FARSITE

5 Anna Movsisyan (2014) Climate change impact on water and temperature conditions of forest soils: A case study related to the Swedish forestry sector

6 Liliana Carolina Castillo Villamor (2015) Technical assessment of GeoSUR and comparison with INSPIRE experience in the context of an environmental vulnerability analysis using GeoSUR data

7 Hossein Maazallahi (2015) Switching to the "Golden Age of Natural Gas" with a Focus on Shale Gas Exploitation: A Possible Bridge to Mitigate Climate Change?

8 Mohan Dev Joshi (2015) Impacts of Climate Change on *Abies spectabilis*: An approach integrating Maxent Model (MAXent) and Dynamic Vegetation Model (LPJ-GUESS)

9 Altaaf Mechiche-Alami (2015) Modelling future wheat yields in Spain with LPJ-GUESS and assessing the impacts of earlier planting dates

10 Koffi Unwana Saturday (2015) Petroleum activities, wetland utilization and livelihood changes in Southern Akwa Ibom State, Nigeria: 2003-2015

11 José Ignacio Díaz González (2016) Multi-objective optimisation algorithms for GIS-based multi-criteria decision analysis: an application for evacuation planning

12 Gunjan Sharma (2016) Land surface phenology as an indicator of performance of conservation policies like Natura2000

13 Chao Yang (2016) A Comparison of Four Methods of Diseases Mapping

14 Xinyi Dai (2016) Dam site selection using an integrated method of AHP and GIS for decision making support in Bortala, Northwest China

15 Jialong Duanmu (2016) A multi-scale based method for estimating coniferous forest aboveground biomass using low density airborne LiDAR data

16 Tanyaradzwa J. N. Muswera (2016) Modelling maize (Zea Mays L.) phenology using seasonal climate forecasts

17 Maria Angela Dissegna (2016) Improvement of the GPP estimations for Sudan using the evaporative fraction as water stress factor

18 Miguel G. Castro Gómez (2017) Joint use of Sentinel-1 and Sentinel-2 for land cover classification: A machine learning approach

19 Krishna Lamsal (2017) Identifying potential critical transitions in a forest ecosystem using satellite data

20 Maimoona Zehra Jawaid (2017) Glacial lake flood hazard assessment and modelling: a GIS perspective

21 Tracy Zaarour (2017) Application of GALDIT index in the Mediterranean region to assess vulnerability to sea water intrusion

22 Stephania Zabala (2017) Comparison of multi-temporal and multispectral Sentinel-2 and UAV (unmanned aerial vehicle) imagery for crop type mapping

23 Ximena Tagle (2017) Radiometric calibration of unmanned aerial vehicle remote sensing imagery for vegetation mapping

24 Tesfaye Gebeyehu Admasu (2017) Monitoring trends of greenness and LULC (land use/land cover) in Addis Ababa and its surrounding using MODIS time-series and LANDSAT data

25 Haiqi Xu (2017) Development of a digitalization tool for linking thematic data to a background map

26 Zeyao Zhang (2018) BIM to GIS-based building model conversion in support of urban energy simulation

27 Aiman Shahpurwala (2019) Conflict, narratives, and forest fires in eastern Turkey : a quantitative perspective with remote sensing and GIS